Ann. Geophys., 26, 4051–4074, 2008
www.ann-geophys.net/26/4051/2008/

Annales Geophysicae

Axi-symmetric models of auroral current systems in Jupiter's magnetosphere with predictions for the Juno mission

S. W. H. Cowley[1], **A. J. Deason**[1,*], **and E. J. Bunce**[1]

[1]Department of Physics & Astronomy, University of Leicester, Leicester LE1 7RH, UK
[*]currently at: Sidney Sussex College, University of Cambridge, Cambridge CB2 3HU, UK

Received: 10 April 2008 – Revised: 2 September 2008 – Accepted: 20 November 2008 – Published: 12 December 2008

Abstract. We develop two related models of magnetosphere-ionosphere coupling in the jovian system by combining previous models defined at ionospheric heights with magnetospheric magnetic models that allow system parameters to be extended appropriately into the magnetosphere. The key feature of the combined models is thus that they allow direct connection to be made between observations in the magnetosphere, particularly of the azimuthal field produced by the magnetosphere-ionosphere coupling currents and the plasma angular velocity, and the auroral response in the ionosphere. The two models are intended to reflect typical steady-state sub-corotation conditions in the jovian magnetosphere, and transient super-corotation produced by sudden major solar wind-induced compressions, respectively. The key simplification of the models is that of axi-symmetry of the field, flow, and currents about the magnetic axis, limiting their validity to radial distances within $\sim$30 R_J of the planet, though the magnetic axis is appropriately tilted relative to the planetary spin axis and rotates with the planet. The first exploration of the jovian polar magnetosphere is planned to be undertaken in 2016–2017 during the NASA New Frontiers Juno mission, with observations of the polar field, plasma, and UV emissions as a major goal. Evaluation of the models along Juno planning orbits thus produces predictive results that may aid in science mission planning. It is shown in particular that the low-altitude near-periapsis polar passes will generally occur underneath the corresponding auroral acceleration regions, thus allowing brief examination of the auroral primaries over intervals of $\sim$1–3 min for the main oval and $\sim$10 s for narrower polar arc structures, while the "lagging" field deflections produced by the auroral current systems on these passes will be $\sim$0.1°, associated with azimuthal fields above the ionosphere of a few hundred nT.

Correspondence to: S. W. H. Cowley
(swhc1@ion.le.ac.uk)

Keywords. Magnetospheric physics (Auroral phenomena; Magnetosphere-ionosphere interactions; Planetary magnetospheres)

1 Introduction

Much progress has been made in recent years in determining the nature of magnetosphere-ionosphere coupling at Jupiter, a topic of central significance in understanding the properties of its large-scale plasma environment. Observations of auroral phenomena have provided a primary means of investigation, both at ultra violet (UV) wavelengths using the Hubble Space Telescope (HST), and in the infra red (IR) using ground-based telescopes. UV images show with increasing latitude auroral emissions associated with magnetosphere-moon interactions, a relatively steady main oval that dominates the overall auroral power output and maps magnetically to the middle magnetosphere, and spatially structured and variable emissions at highest latitudes in the polar cap (Clarke et al., 1998, 2002, 2004, 2008; Prangé et al., 1998; Pallier and Prangé, 2001, 2004; Waite et al., 2001; Grodent et al., 2003a, b; Nichols et al., 2007). UV spectra have also provided information on the energy of the auroral primary particles, showing that the main oval is produced by precipitating electrons with average energies in the range $\sim$50–150 keV (Gustin et al., 2004, 2006). Doppler observations of IR emissions from ionospheric H_3^+ ions have also shown that the jovian main oval is associated with corotation breakdown of the magnetospheric plasma (Rego et al., 1999; Stallard et al., 2001, 2003).

Theoretical discussion of these auroral emissions has focussed principally on the field-aligned acceleration of magnetospheric electrons into the polar ionosphere in regions of strong upward-directed field-aligned current (Kennel and

Published by Copernicus Publications on behalf of the European Geosciences Union.

Coroniti, 1975; Barbosa et al., 1981), though other studies have proposed a significant role for turbulent processes (Saur et al., 2003). The field-aligned currents form part of a large-scale magnetosphere-ionosphere coupling current system associated with momentum exchange between these regions, communicated via the magnetic field. The current system associated with the main oval is believed to be related to centrifugally-driven outward radial transport of iogenic plasma that leads to sub-corotation in the middle magnetosphere (Hill, 1979, 2001; Huang and Hill, 1989; Cowley and Bunce, 2001; Southwood and Kivelson, 2001; Cowley et al., 2002; Nichols and Cowley, 2003, 2004). In addition, upward-directed field-aligned currents are also expected to flow at the open-closed field line boundary due to the shear between moderately sub-corotating plasma flow on outer closed field lines and strongly sub-corotating plasma flow on open field lines mapping to the tail, which may relate to some emissions poleward of the main oval (Cowley et al., 2003). In particular, it has been suggested that the structured and variable auroras observed near noon poleward of the main oval relate to pulsed reconnection at the cusp magnetopause (Waite et al., 2001; Pallier and Prangé, 2001, 2004; Bunce et al., 2004).

A simple axi-symmetric model of the plasma flow in the jovian system, the related coupling currents, and the consequent auroral precipitation based on these considerations has been proposed by Cowley et al. (2005), intended to represent typical steady-state conditions. This model has also been extended by Cowley et al. (2007) to consider auroral effects resulting from sudden compressions of the magnetosphere, extending earlier work by Cowley and Bunce (2003a, b). Because these studies were directed principally toward understanding observations of auroral emissions and ionospheric flows as outlined above, they principally considered conditions at ionospheric heights, defining, for example, the model zonal plasma flow around the magnetic axis as a function of co-latitude. The principal purpose of this paper is to show how these models can be appropriately extended along model field lines into the magnetosphere, including the effect of the rotation of the magnetic axis about the planet's spin axis, in order to consider their implications for conditions in the magnetosphere and thus relating them to in situ observations from spacecraft. For simplicity, however, we retain the axi-symmetric approximation about the magnetic axis, thus limiting the region of approximate validity of the model to radial distances within $\sim 30\,R_J$. While the field-aligned coupling currents continue to form a central focus of consideration, they are too weak to measure directly in magnetospheric plasma particle data. However, they produce a readily-observable magnetic signature via the presence of azimuthal fields that bend the field lines out of magnetic meridians (e.g. Khurana, 2001, and references therein). This field therefore represents a key observable in magnetospheric data, along with the plasma angular velocity. The azimuthal fields produced by the auroral current system in the Cowley et al. (2005, 2007) models have not previously been computed, but will be evaluated here throughout the region between the ionosphere and the magnetospheric equatorial plane. With regard to relevant observations, we note that most jovian magnetospheric data to date have been acquired close to the equatorial plane (excepting the outbound passes of Pioneer-11 and Ulysses at intermediate latitudes), including all the data from the Voyager and Galileo missions (e.g. Dessler, 1983; Khurana, 2001; Krupp et al., 2001; Frank et al., 2002). The first true polar observations of auroral plasma and fields at Jupiter are planned as part of the forthcoming NASA New Frontiers Juno mission. Here we therefore illustrate our results by evaluation of model parameters along Juno planning trajectories, the results thus forming potential aids to Juno mission planning.

2 Theoretical basis of the model

We begin by outlining the nature of the jovian models proposed by Cowley et al. (2005, 2007), and the considerations on which they are based. The principal model assumptions are that the field and flow is steady-state and axi-symmetric about the magnetic axis, these leading to great simplifications of analysis. Consequently, however, the model is unable to represent effects associated with dynamic local time-dependent phenomena such as the dayside cusp near noon and substorm-like processes on the nightside (e.g. Pallier and Prangé, 2001, 2004; Woch et al., 2002), nor can it describe the averaged dawn-dusk flow asymmetry observed in equatorial particle data that leads to weakened coupling currents and auroras in the pre-noon sector (Krupp et al., 2001; Woch et al., 2004; Radioti et al., 2008). Nevertheless, the model provides a useful initial description of the central region of the rotation-dominated jovian magnetosphere, and also serves to illustrate that even a relatively simple model leads to predicted complexity of in situ observations. With these assumptions, then, the nature of the calculation is relatively simple. An empirical model of the plasma angular velocity about the magnetic axis is first constructed, based on observations, model results, and theoretical considerations. This is then combined with ionospheric parameters to determine the meridional height-integrated Pedersen current flowing in the ionosphere, from which the field-aligned current density flowing on field lines above the ionosphere is obtained by calculating its divergence. The field perturbations above the ionosphere produced by the coupling current system consisting of the Pedersen currents, field-aligned currents, and magnetospheric closure currents, can then be found from Ampère's law, while the auroral acceleration parameters are determined from Knight's (1973) kinetic theory.

In somewhat more detail, in the work presented here the jovian Pedersen conducting layer is taken to be a surface located $\sim$500 km above the 1 bar atmospheric pressure level (Millward et al., 2002), which itself lies at a polar radius of

66 854 km. Since we are interested only in the sub-corotating plasma region within ∼25° co-latitude of each magnetic pole, we can thus take this surface to be a sphere of radius R_i=67 350 km, neglecting the polar-flattened figure of the planet. While this assumption is in common with Cowley et al. (2005, 2007), the latter authors also assumed a uniform radial ionospheric magnetic field of strength 1.1 mT. However, this assumption is unsuitable here, since we wish to map plasma parameters along field lines between the ionosphere and magnetosphere, and thus need to adopt a simple model of the planetary field extending away from Jupiter. The simplest reasonably realistic internal field for this purpose is a dipole field that is tilted with respect to the planet's spin axis, whose properties are determined here from the dipole coefficients of the VIP4 empirical model of Connerney et al. (1998). In this case the magnetic dipole (subscript "D") axis is tilted through an angle of θ'_D=9.515° relative to the planet's spin axis, and the field components and flux function are given by

$$B_{D\,r} = 2g\cos\theta\left(\frac{R_J}{r}\right)^3 \tag{1a}$$

and

$$B_{D\,\theta} = g\sin\theta\left(\frac{R_J}{r}\right)^3 \tag{1b}$$

and

$$F_D = gR_J^2\sin^2\theta\left(\frac{R_J}{r}\right) \quad , \tag{2}$$

where r and θ are spherical polar coordinates referenced to the northern magnetic axis. The internal azimuthal field about this axis is, of course, zero. In these expressions R_J is Jupiter's conventional radius equal to 71 323 km, and dipole coefficient g=426 366 nT using the VIP4 model. We note that the ionospheric field strength at the magnetic pole is then given by $2g\left(R_J/R_i\right)^3$=1.012 mT, which thus differs only marginally from the value employed in the previous related studies. This value is also representative of typical polar field strengths in the VIP4 model (see e.g. Plate 2 of Connerney et al., 1998). The flux function $F\,(r,\ \theta)$ for an axi-symmetric field is related to the field components by $B=\left(1/r\sin\theta\right)\nabla F\times\hat{\varphi}$, where $\hat{\varphi}$ is the unit vector in the azimuthal direction around the axis, such that F is constant on a field line. This function is thus employed to map field lines between the ionosphere and magnetosphere. Within the magnetosphere the field and flux function values are augmented by an additional contribution from the middle magnetosphere current sheet, as will be described below, but this is neglected in the ionosphere where the field is overwhelmingly dominated by the planetary field.

We then assume that in the planet's rest frame the plasma at ionospheric heights (in the absence of collisions) rotates about the magnetic axis with angular frequency $\Delta\omega_i\,(\theta_i)$, where θ_i is the co-latitude referenced to the northern magnetic axis (as above). The value of $\Delta\omega_i$ is taken to be positive when the flow is in the $-\hat{\varphi}$ direction, i.e. positive when directed clockwise as viewed from above the north magnetic pole. The condition $\Delta\omega_i$=0 then corresponds to rigid corotation, while $\Delta\omega_i$ positive represents sub-corotation of the plasma relative to the planet, with $\Delta\omega_i=\Omega_J$ indicating non-rotation of the plasma in the inertial frame. Here $\Omega_J\approx1.758\times10^{-4}\,\mathrm{rad\,s^{-1}}$ is the angular frequency of planetary rotation, corresponding to a rotation period of ∼9.93 h. The same plasma angular velocity about the magnetic axis is then applies to the whole magnetospheric flux shell mapping to the ionosphere at co-latitude θ_i, as required by the assumption of a temporally invariant axi-symmetric magnetic field. Due to the assumed symmetry of the planetary (and total) field about the magnetic equator, the model plasma angular velocity is also symmetric about the equator (certainly on closed magnetospheric flux shells), and thus has the same co-latitude profile with respect to the magnetic pole in both hemispheres. We also assume that the drag on the neutral atmosphere within the Pedersen layer due to ion-neutral collisions induces a similar differential rotation of the neutral atmosphere in the layer, which is a factor k times the ion differential angular velocity $\Delta\omega_i$, where $0<k<1$. Atmospheric sub-corotation about the magnetic axis is unlikely to be a very realistic assumption due e.g. to the effect of the Coriolis force on the motion of the neutral gas, but this assumption is the only way to include such drag effects in an axi-symmetric model.

With these assumptions the plasma velocity within the ionospheric Pedersen layer relative to the neutral gas is

$$\boldsymbol{V}'_i\,(\theta_i) = -\,(1-k)\ R_i\sin\theta_i\ \Delta\omega_i\,(\theta_i)\ \hat{\boldsymbol{\varphi}} \quad . \tag{3}$$

The electric field in the neutral atmosphere rest frame is then $\boldsymbol{E}'_i\,(\theta_i)=-\boldsymbol{V}'_i\,(\theta_i)\times\boldsymbol{B}_{Di}\,(\theta_i)$, where $\boldsymbol{B}_{Di}$ is the planetary dipole field given by Eq. (1) evaluated in the Pedersen layer, and the ionospheric Pedersen current density then follows from $\boldsymbol{j}_P\,(\theta_i)=\sigma_P\boldsymbol{E}'_i\,(\theta_i)$, where σ_P is the ionospheric Pedersen conductivity. We note, however, that because the magnetic field is not exactly vertical except at the magnetic pole, the Pedersen current has both meridional and small radial components, these corresponding to the local horizontal and vertical respectively. To ensure that the total current has only a meridional (i.e. horizontal) component we assume that a small field-aligned current flows in the Pedersen layer which is such that the vertical current is reduced identically to zero, thus also slightly augmenting the meridional current. With this assumption, and integrating in height through the Pedersen layer, the meridional horizontal Pedersen current intensity flowing in the ionosphere is

$$i_{hP}\,(\theta_i) = \Sigma_P^*\ R_i\sin\theta_i\ \Delta\omega_i\,(\theta_i)\,|B_{Di\,r}\,(\theta_i)|\ f\,(\theta_i) \quad , \tag{4}$$

defined as positive when directed equatorward in both hemispheres. In this expression Σ_P^* is the effective

height-integrated Pedersen conductivity taking account of the slippage of the neutral atmosphere as described above, given in terms of the actual height-integrated conductivity Σ_P by $\Sigma_P^* = (1-k)\,\Sigma_P$. Function $f \approx 1$ is the factor that takes account of the non-vertical field, given by

$$f\,(\theta_i) = 1 + \left(\frac{B_{Di\,\theta}}{B_{Di\,r}}\right)^2 = 1 + \frac{1}{4}\tan^2\theta_i \quad , \tag{5}$$

where use has been made of Eq. (1). We then integrate this current in azimuth around the magnetic axis to find the total meridional horizontal Pedersen current at co-latitude θ_i

$$\begin{aligned} I_{hP}\,(\theta_i) &= 2\pi R_i \sin\theta_i i_{hP}\,(\theta_i) \\ &= 2\pi\,\Sigma_P^* R_i^2 \sin^2\theta_i\,\Delta\omega_i\,(\theta_i)\,|B_{Di\,r}\,(\theta_i)|\,f\,(\theta_i)\,, \end{aligned} \tag{6}$$

again defined as positive when directed equatorward in both hemispheres. Current continuity then requires the field-aligned current density just above the ionosphere to be given by

$$j_{\mathrm{FAC}\,i}\,(\theta_i) = -\,\frac{1}{2\pi R_i^2 \sin\theta_i}\,\frac{B_{Di}\,(\theta_i)}{B_{Di\,r}\,(\theta_i)}\,\left(\frac{dI_{hP}}{d\theta_i}\right) \quad , \tag{7}$$

where $B_{Di}\,(\theta_i) = \sqrt{B_{Di\,r}^2 + B_{Di\,\theta}^2}$ is the total field strength in the Pedersen layer, and $j_{\mathrm{FAC}\,i}$ has been defined such that positive values indicate currents directed outward from the planet (in both hemispheres), while negative values indicate currents directed inward. The corresponding field-aligned current density in the magnetosphere at a point where the field strength is B and maps to the ionosphere at co-latitude θ_i is then given from current continuity by

$$j_{\mathrm{FAC}} = \frac{B}{B_{Di}}\,j_{\mathrm{FAC}\,i}\,(\theta_i) \quad . \tag{8}$$

This formula applies to all points along a field line between the ionosphere and the region where the currents close across the field lines in the magnetosphere. On closed middle magnetosphere field lines this current closure region corresponds to the equatorial plasma disk.

While the above discussion has focussed on the Pedersen currents, we note that plasma sub-corotation will also drive azimuthal Hall currents eastward in the model ionosphere. However, in the axi-symmetric approximation these close wholly in the ionosphere and do not contribute to the field-aligned current density of primary interest here.

We now consider the magnetic field produced by the combined coupling current circuit consisting of the ionospheric Pedersen current, the field-aligned current, and the magnetospheric closure current. It is evident from the geometry of this solenoidal current system that the related field perturbations are purely azimuthal and contained inside the region of the current loops. To find this field a point at radius r and magnetic co-latitude θ between the ionosphere and the closure currents in the equatorial plane we apply Ampère's law to a circular path of radius $\rho = r\sin\theta$ around the magnetic axis passing through the point, where ρ is the perpendicular distance from the magnetic axis. It is evident that the total current passing through the surface bounded by this loop is just the total Pedersen current flowing in the ionosphere at the feet of the field lines passing through the point, corresponding to ionospheric co-latitude θ_i. The azimuthal field is then given by

$$B_\varphi\,(r,\ \theta) = \mp\frac{\mu_o}{2\pi\ \rho}\ I_{hP}\,(\theta_i) \quad , \tag{9}$$

where the upper sign corresponds to the Northern Hemisphere and the lower to the Southern (and I_{hP} is positive equatorward in both hemispheres as above). The peak B_φ on each field line occurs just above the ionosphere, whose value $B_{\varphi i}\,(\theta_i)$ can be obtained from Eq. (9) by putting $\rho = R_i \sin\theta_i$. Alternatively we can apply Ampère's law directly to the ionospheric current layer, noting that the azimuthal field is zero underneath the layer, to obtain

$$B_{\varphi i}\,(\theta_i) = \mp\mu_o\ i_{hP}\,(\theta_i) = \mp\frac{\mu_o}{2\pi\ R_i \sin\theta_i}\ I_{hP}\,(\theta_i) \quad , \tag{10}$$

where i_{hP} is the horizontal Pedersen current intensity given by Eq. (4).

We are also interested in the auroral acceleration parameters implied by the above field-aligned currents. In particular, in relation to the Juno mission, we wish to know whether the spacecraft is likely to fly above or below the low-altitude electron acceleration regions, and in the latter case what the energy of the auroral primaries is likely to be. In common with previous studies, we estimate these quantities using Knight's (1973) kinetic theory, which we now briefly summarise. If the magnetospheric source populations are described as isotropic Maxwellians of density N and thermal energy W_{th} (equal to kT), then the maximum current density and energy flux that can be deposited in the ionosphere without field-aligned electron acceleration are given by

$$j_{\mathrm{FAC}\,0} = eN\left(\frac{W_{th}}{2\pi m_e}\right)^{1/2} \tag{11a}$$

and

$$E_{f0} = 2NW_{th}\left(\frac{W_{th}}{2\pi m_e}\right)^{1/2}, \tag{11b}$$

where e and m_e are the electron charge and mass respectively. These formulas correspond to the case of a full downward-going loss-cone, and an empty upward-going loss-cone. If the required upward current density is larger than $j_{\mathrm{FAC}\,0}$, then a field-aligned voltage must be present to accelerate the source electrons into the ionosphere, the minimum value of which for upward current $j_{\mathrm{FAC}\,i} \geq j_{\mathrm{FAC}\,0}$ is given by Knight's (1973) theory as

$$\Phi_{||\,\min} = \frac{W_{th}}{e}\left[\left(\frac{j_{\mathrm{FAC}\,i}}{j_{\mathrm{FAC}\,0}}\right) - 1\right] \quad . \tag{12}$$

This value is appropriate if the "top" of the voltage drop is located at a radial distance well above the minimum value given by

$$\left(\frac{r_{\min}}{R_i}\right) \approx \left(\frac{j_{\mathrm{FAC}\,i}}{j_{\mathrm{FAC}\,0}}\right)^{1/3} \quad . \tag{13}$$

Following Lundin and Sandahl (1978), the enhanced precipitating electron energy flux corresponding to Eq. (12) is then given by

$$E_f = \frac{E_{f0}}{2}\left[\left(\frac{j_{\mathrm{FAC}\,i}}{j_{\mathrm{FAC}\,0}}\right)^2 + 1\right] \quad . \tag{14}$$

The values of the source electron density and thermal energy employed in various regions of the model, and the consequent limiting currents and energy densities, will be discussed below in Sect. 3 where the specifics of the model are outlined.

We note in relation to this aspect of the model that the field-aligned voltages given by Eq. (12) are typically tens of kV in the jovian context, as will be shown below, much smaller than the voltages associated with the field-transverse flows in the middle and outer magnetosphere, of order several MV. Consequently, in common with previous works, we do not include their effect in modifying the flow mapping between the magnetosphere and ionosphere.

3 Model for steady state conditions

3.1 Flows and currents in the ionosphere

In this section we consider the model proposed by Cowley et al. (2005), representing typical near-steady flow conditions in the jovian magnetosphere, though we use slightly modified parameters to ensure compatibility with the magnetospheric magnetic model introduced in Sect. 3.2 below. The model angular velocity about the magnetic axis in the inertial frame, $\omega_i\,(\theta_i)$, related to the differential rotation in the planetary rest frame $\Delta\omega_i\,(\theta_i)$ by $\omega_i\,(\theta_i) = \Omega_J - \Delta\omega_i\,(\theta_i)$, is given by

$$\begin{aligned}\left(\frac{\omega_i\,(\theta_i)}{\Omega_J}\right) = &\left(\frac{\omega_i}{\Omega_J}\right)_O \\ &+\left[\left(\frac{\omega_i}{\Omega_J}\right)_{OM} - \left(\frac{\omega_i}{\Omega_J}\right)_O\right]\left[\frac{1}{2}\left(1+\tanh\left(\frac{\theta_i-\theta_{iO}}{\Delta\theta_{iO}}\right)\right)\right] \\ &+\left[1-\left(\frac{\omega_i}{\Omega_J}\right)_{OM}\right]\left[\frac{1}{2}\left(1+\tanh\left(\frac{\theta_i-\theta_{iMM}}{\Delta\theta_{iMM}}\right)\right)\right]\end{aligned} \tag{15}$$

This formula applies specifically to the Northern Hemisphere ($0 \le \theta_i \le 90°$), and is mirrored about the magnetic equator so that the overall angular velocity profile is symmetric, as indicated above. The model parameters in Eq. (15) define the plasma angular velocity $\left(\omega_i/\Omega_J\right)_O$ on open field lines at highest latitudes, its transition to the outer magnetosphere value $\left(\omega_i/\Omega_J\right)_{OM}$ across the open-closed field line boundary at $\theta_i = \theta_{iO}$ in a layer of width $\sim 3\Delta\theta_{iO}$ that defines the latitudinal extent of the field-aligned currents flowing in the boundary, and then the transition to near-rigidly corotating flow across the middle magnetosphere region mapping to a layer of width $\sim 3\Delta\theta_{iMM}$ centred on $\theta_i = \theta_{iMM}$. With a few minor modifications compared with Cowley et al. (2005), the values of these parameters employed here are $\left(\omega_i/\Omega_J\right)_O = 0.1$, $\left(\omega_i/\Omega_J\right)_{OM} = 0.35$, $\theta_{iO} = 10.716°$, $\Delta\theta_{iO} = 0.125°$, $\theta_{iMM} = 16.1°$, and $\Delta\theta_{iMM} = 0.5°$, determined from a combination of theoretical studies, Voyager and Galileo observations, and modelling (e.g. Acuña et al., 1983; Isbell et al., 1984; Kane et al., 1995; Krupp et al., 2001; Nichols and Cowley, 2003, 2004). We note that the model angular velocity on open field lines is the same as that of Cowley et al. (2005), while for definiteness the normalised value in the outer magnetosphere, 0.35, has been taken to be intermediate between the two values, 0.25 and 0.5, employed in the latter study. We also note that the value of θ_{iO} is such that the polar cap contains 500 GWb of open magnetic flux as in Cowley et al. (2005), while the position θ_{iMM} and width $\sim 3\Delta\theta_{iMM}$ of the middle magnetosphere layer have been slightly adjusted to ensure that this layer maps magnetically into the model middle magnetosphere equatorial current sheet, as demonstrated in Sect. 3.2 below. With these values, the model angular velocity profile in the northern ionosphere is plotted versus co-latitude θ_i in Fig. 1a. It can be seen that the flow strongly sub-corotates on open field lines, increases sharply to intermediate values in the outer magnetosphere across the open-closed field line boundary at 10.716°, and then to near-rigid corotation conditions in the inner magnetosphere across the middle magnetosphere layer which has a width of $\sim 1.5°$ in the ionosphere centred on $\sim 16.1°$.

Figure 1b and c shows the currents driven by this flow system, specifically the azimuth-integrated horizontal ionospheric Pedersen current, and the field-aligned current density just above the ionosphere, given by Eqs. (6) and (7) respectively. Here we have used an effective ionospheric Pedersen conductivity of $\Sigma_P^* = 0.25$ mho, slightly higher than the value of 0.2 mho employed by Cowley et al. (2005), such that the currents are comparable with the latter study despite the slightly weaker model ionospheric magnetic field. In Fig. 1b it can be seen that the Pedersen current increases with co-latitude to peak at ~ 30 MA at the boundary between open and closed field lines, falls by ~ 6 MA at this boundary as the angular velocity rises towards corotation, rises further across the outer magnetosphere to peak at ~ 45 MA near the boundary with the middle magnetosphere, and then falls rapidly across the latter region as the flow rises to rigid corotation. The field-aligned currents in Fig. 1c are correspondingly directed downward (negative) in regions where the azimuth-integrated Pedersen current increases with co-latitude, and upward (positive) in regions where it decreases with co-latitude. Relatively weak downward currents $\sim 50\,\mathrm{nA\,m^{-2}}$ thus flow into the ionosphere in the region of open field lines and in the outer magnetosphere, while relatively strong

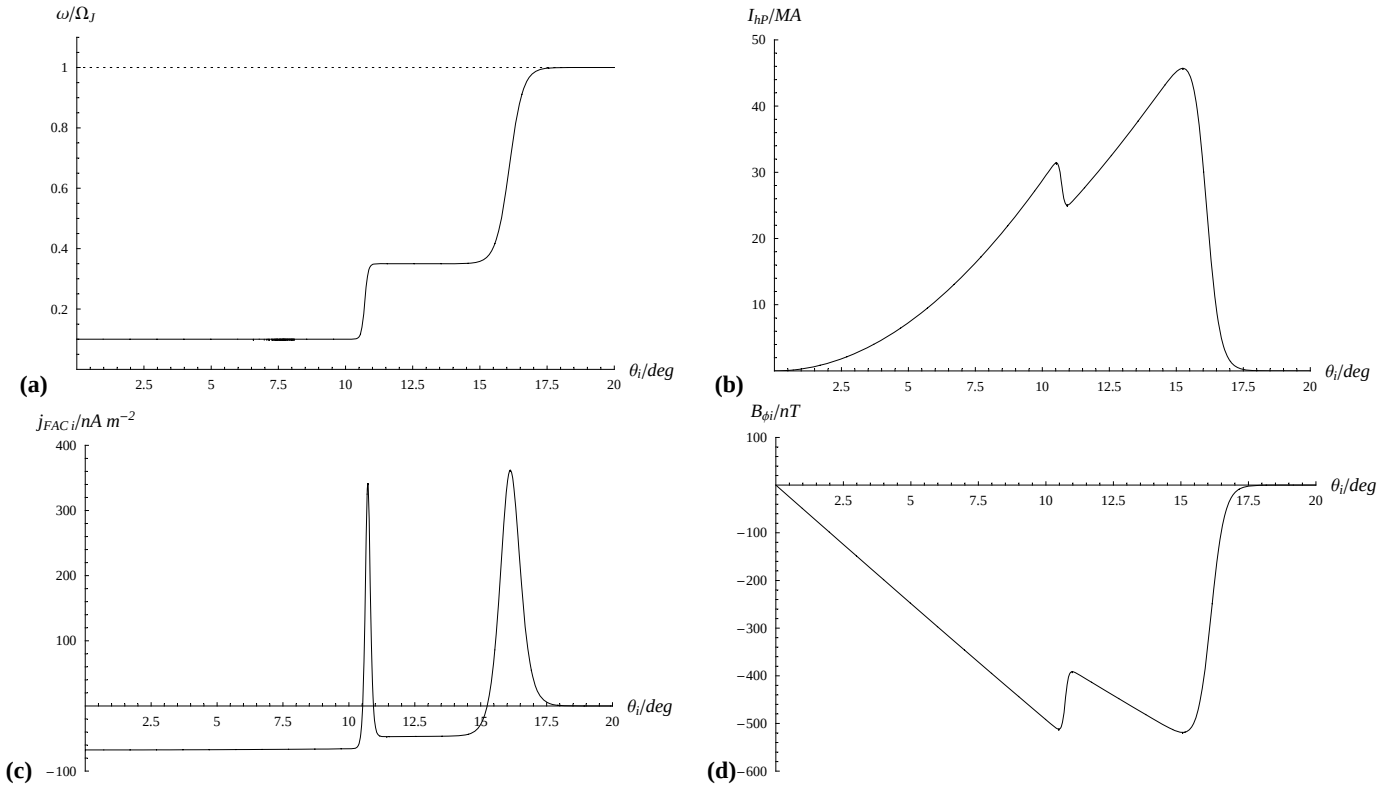

Fig. 1. Plasma flow and current system representative of steady-state conditions in the jovian system, based on Cowley et al. (2005), plotted versus co-latitude θ_i in the northern high-latitude ionosphere. The panels of the figure show **(a)** the plasma angular velocity normalised to the planet's angular velocity given by Eq. (15), where rigid corotation is indicated by the horizontal dotted line, **(b)** the azimuth-integrated horizontal Pedersen current flowing equatorward in the ionosphere given by Eq. (6), **(c)** the field-aligned current density just above the ionosphere required by the divergence of the Pedersen current given by Eq. (7), where positive values indicate upward currents and negative values downward currents, and **(d)** the azimuthal field just above the northern ionosphere produced by the magnetosphere-ionosphere coupling current system given by Eq. (10).

upward currents peaking at $\sim$350 nA m^{-2} flow in narrow layers at the open-closed field line boundary and across the middle magnetosphere layer.

The azimuthal field just above the ionosphere produced by these currents, not previously computed by Cowley et al. (2005), is shown in Fig. 1d, obtained from Eqs. (9) or (10). Its value is negative throughout the northern high latitude region shown, corresponding to a "lagging" tilt in the field caused by ion-neutral collisions in the Pedersen layer in the presence of sub-corotation. Its magnitude grows with co-latitude to $\sim$500 nT near the open-closed field line boundary, then falls by $\sim$100 nT at this boundary as the plasma angular velocity increases, associated with the layer of upward-directed field-aligned current in the boundary. The field magnitude then grows once more to $\sim$500 nT across the outer magnetosphere region, before falling rapidly to zero across the middle magnetosphere as the plasma angular velocity rises, in association with the upward-directed field-aligned current in the layer. We note, however, that the peak azimuthal field of $\sim$500 nT corresponds to only $\sim$0.05% of the planetary field in the ionosphere, such that the field tilts out of dipole meridian planes above the ionosphere through peaks angles of only $\sim$0.03°.

To examine the consequences of the upward currents for auroral acceleration we must first define the source electron parameters to be employed in Eqs. (11–14). These are given in Table 1, where for simplicity we use three sets of constant values based on Voyager and Galileo data, that are taken to be characteristic of the three main regions of our model (Cowley et al., 2005). These are dense cool magnetosheath plasma (0.5 cm^{-3} and 50 eV) on open field lines, warm tenuous plasma (0.02 cm^{-3} and 250 eV) in the outer magnetosphere, and hot tenuous plasma (0.01 cm^{-3} and 2.5 keV) in the middle magnetosphere. The source parameters switch from magnetosheath to outer magnetosphere values across the open-closed field boundary at $\theta_i = \theta_{iO}$, and between outer magnetosphere and middle magnetosphere values at the poleward boundary of the middle magnetosphere layer, taken to lie at a co-latitude of $\theta_i = \theta_{iMM} - 2\Delta\theta_{iMM} = 15.1°$ (relative to either pole). In practice, therefore, the magnetosheath and outer

Table 1. Properties of the magnetospheric source electron parameters employed in auroral calculations.

Parameter	Magnetosheath	Outer magnetosphere	Middle magnetosphere
Electron density N (cm^{-3})	0.5	0.02	0.01
Electron thermal energy W_{th} (keV)	0.05	0.25	2.5
Unaccelerated current density $j_{FAC\,0}$ ($nA\,m^{-2}$)	94.8	8.48	13.4
Unaccelerated energy flux E_{f0} ($\mu W\,m^{-2}$)	9.48	4.24	67.0

magnetosphere source parameters are applied only in the upward current regions lying immediately poleward and equatorward of the open-closed field line boundary, respectively, while the middle magnetosphere source parameters are applied uniformly across the upward current region mapping to the middle magnetosphere. Also noted in Table 1 are the values of the unaccelerated field-aligned current densities and energy fluxes carried by these populations, given by Eq. (11). On the basis that $1\,mW\,m^{-2}$ of precipitating electrons produces a UV auroral emission of ∼10 kR, it can be seen that unaccelerated precipitation of these populations will give rise to emissions typically in the range ∼0.1–1 kR, below the few kR level of present detectability, and much less than typical jovian main oval and polar emission intensities of several tens to several hundreds of kR (e.g. Grodent et al., 2003a, b). It can also be seen, however, that the maximum field-aligned current density that can be provided by these unaccelerated populations are all less than the peak upward field-aligned current densities required by the model, by more than an order of magnitude for the tenuous magnetospheric populations, thus requiring significant field-aligned acceleration of these electrons.

The resulting acceleration parameters are shown in Fig. 2, where Fig. 2a again shows the model field-aligned current density, but now on an expanded scale that spans the model region of upward currents. The corresponding minimum field-aligned acceleration voltage given by Eq. (12) is shown in Fig. 2b. At the open-closed field line boundary the voltage on the poleward side of the boundary peaks at ∼100 V where the current is taken to be carried by magnetosheath electrons, while on the equatorward side where it is carried by outer magnetosphere electrons the voltage peaks at ∼10 kV. Voltages of similar order are also present throughout the middle magnetosphere layer, peaking at ∼65 kV at the centre of the layer. The corresponding precipitating electron energy flux given by Eq. (14) is shown in Fig. 2c. Significant energy fluxes occur only on the equatorward side of the open-closed field line boundary in a layer of ∼0.1° (∼100 km) width where the current is taken to be carried by outer magnetosphere electrons, peaking at the boundary at $\sim 3\,mW\,m^{-2}$. This precipitation would thus give rise to a ∼100 km-wide auroral arc at the boundary at ∼11° colatitude with a peak emission intensity of ∼30 kR. By comparison, electron acceleration in the middle magnetosphere region results in significant precipitating energy fluxes in a layer ∼1° (∼1000 km) wide at ∼16°, peaking at its centre at $\sim 25\,mW\,m^{-2}$ corresponding to a UV emission of ∼250 kR. This precipitation is therefore taken to correspond to the jovian main oval, while that at the open-closed field line boundary is taken to be representative of arcs in the poleward region.

In Fig. 2d we show the minimum radial distance of the field-aligned acceleration regions along the high-latitude field lines given by Eq. (13). For the magnetosheath source the acceleration region can be located quite close to the planet, above a radial distance of $\sim 1.5\,R_J$, due to the modest factor through which the precipitating flux must be augmented. For both magnetospheric source populations, however, the acceleration regions must be located quite high up along the auroral field lines, typically at radial distances exceeding ~ 2–$3\,R_J$.

3.2 Flows and fields in the magnetosphere

We now take the flow and current models defined above in the ionosphere and determine their consequences for magnetospheric observations, obtained by mapping along model magnetic field lines into the magnetosphere. For this purpose we require a reasonably realistic model of the magnetospheric field that includes not only the planetary field, but also the effect of the equatorial current sheet that extends the field lines outward from the planet in the middle magnetosphere. Here for typical steady-state conditions we employ the VIP4 planetary dipole field given by Eqs. (1) and (2) combined with the field of the model equatorial current sheet proposed by Connerney et al. (1981). In this model the current region is a cylindrically-symmetric disc of half-thickness D centred on the magnetic equator, with inner and outer edges at perpendicular distances from the magnetic axis of R_1 and R_2, respectively, within which the azimuthal current density is given by

$$j_\varphi(\rho) = \frac{I_o}{\rho} \quad , \tag{16}$$

where I_o is a constant with SI units of $A\,m^{-1}$, and ρ is again the perpendicular distance from the magnetic axis. In general, the axi-symmetric flux function and poloidal fields produced by this current disc, which we denote by $F_{CAN}(r,\ \theta)$

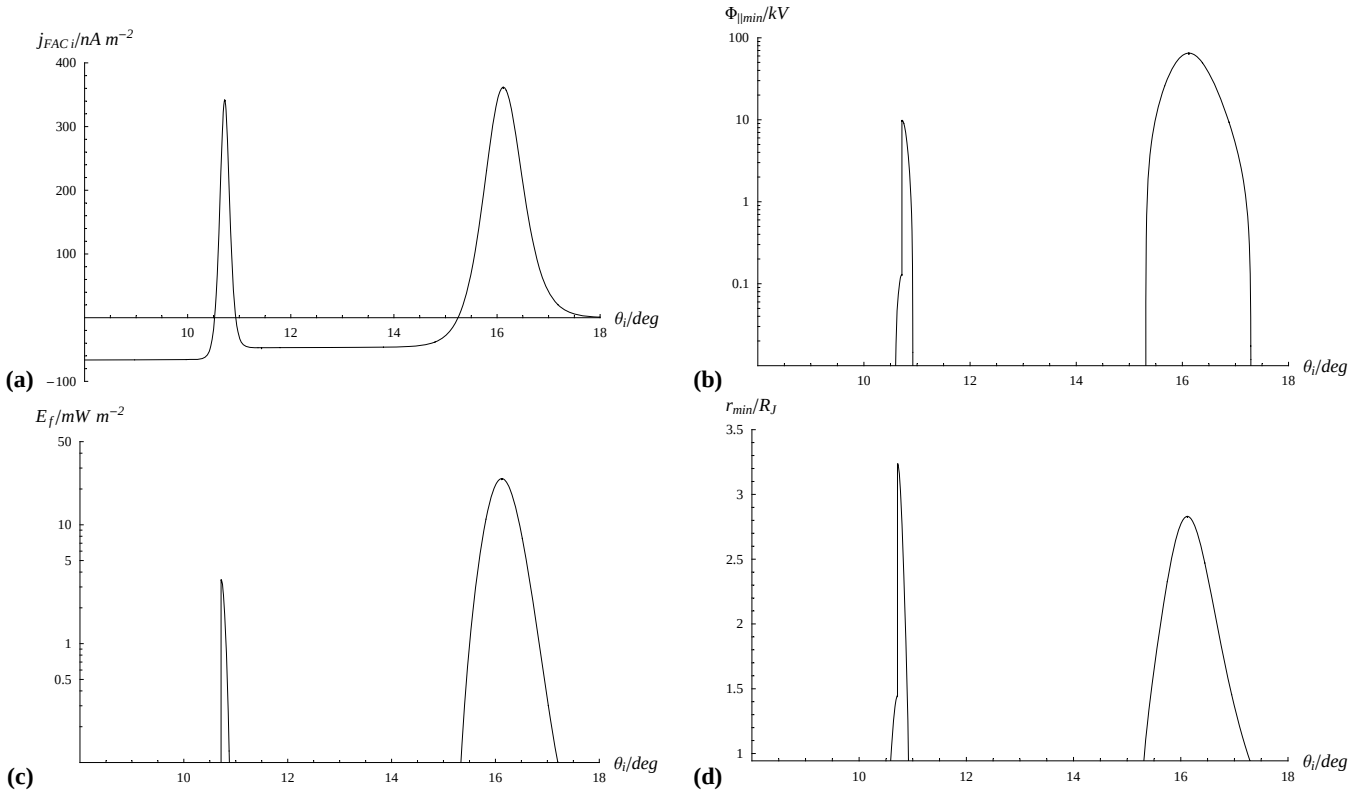

Fig. 2. Auroral acceleration parameters in the upward field-aligned current regions shown in Fig. 1, representative of steady-state conditions in the jovian system. The panels of the figure show **(a)** the field-aligned current density as in Fig. 1c but now on an expanded co-latitude scale, **(b)** the minimum field-aligned acceleration voltage given by Eq. (12), **(c)** the corresponding energy flux of the accelerated electrons given by Eq. (14), and **(d)** the minimum radial distance along the field lines of the field-aligned acceleration regions given by Eq. (13). The properties of the magnetospheric source electrons are those given in Table 1, as discussed in the text.

and $B_{\rm CAN}\,(r,\ \theta)$, must be obtained numerically by evaluation of the integral expression given by Connerney et al. (1981). However, excellent analytic approximations for these quantities have been determined by Edwards et al. (2001), and are employed in the calculations presented here. Connerney et al. (1981) determined best-fit values for the model parameters by comparison with data from the Voyager-1 and -2 fly-bys. They found good fits within radial distances of $\sim$30 R_J using R_1=5 R_J, R_2=50 R_J, and D=2.5 R_J, with $\mu_o I_o$=450 nT for Voyager 1 and 300 nT for Voyager 2. Here we have re-visited the values of these parameters with regard also to the modelling results of Khurana (1997) and the Galileo field data presented by Khurana (2001), and find that the slightly modified parameter set R_1=5.25 R_J, R_2=60 R_J, D=2.5 R_J, and $\mu_o I_o$=350 nT gives a good overall description of the data, which we thus employ in the present study. The model is again taken to apply to radial distances within $\sim$30 R_J from the planet, beyond which the effects of solar wind-induced current sheet hinging and tilting lag have to be taken into account (Khurana, 1997; Khurana and Schwarzl, 2005).

In Fig. 3 we show parameters of the steady-state model mapped from the ionosphere to the equatorial plane using the above magnetic model. Figure 3a shows the model field in the equatorial plane, B_θ, plotted versus radial distance to 30 R_J. The dashed line shows the planetary dipole field alone, falling as the inverse cube of the distance, while the solid line shows the total field, which is everywhere reduced in strength compared with the dipole due to the stretching of the equatorial field lines by the equatorial current disk. The modified mapping from the equatorial plane to the ionosphere is shown in Fig. 3b, where we plot the co-latitude θ_i of the foot of the field line in the ionosphere (with respect to either pole) versus equatorial radial distance. This has been obtained from the constancy of the flux function along each field line, such that from Eq. (2) we have for a general point $(r,\ \theta)$ within the magnetosphere

$$gR_J^2 \sin^2\theta_i \left(\frac{R_J}{R_i}\right) = gR_J^2 \sin^2\theta \left(\frac{R_J}{r}\right) + F_{\rm CAN}\,(r,\theta)\,, \quad (17)$$

where the small effect of the current sheet field has been neglected in the ionosphere. The dashed line in Fig. 3b again corresponds to the dipole field alone for purposes of

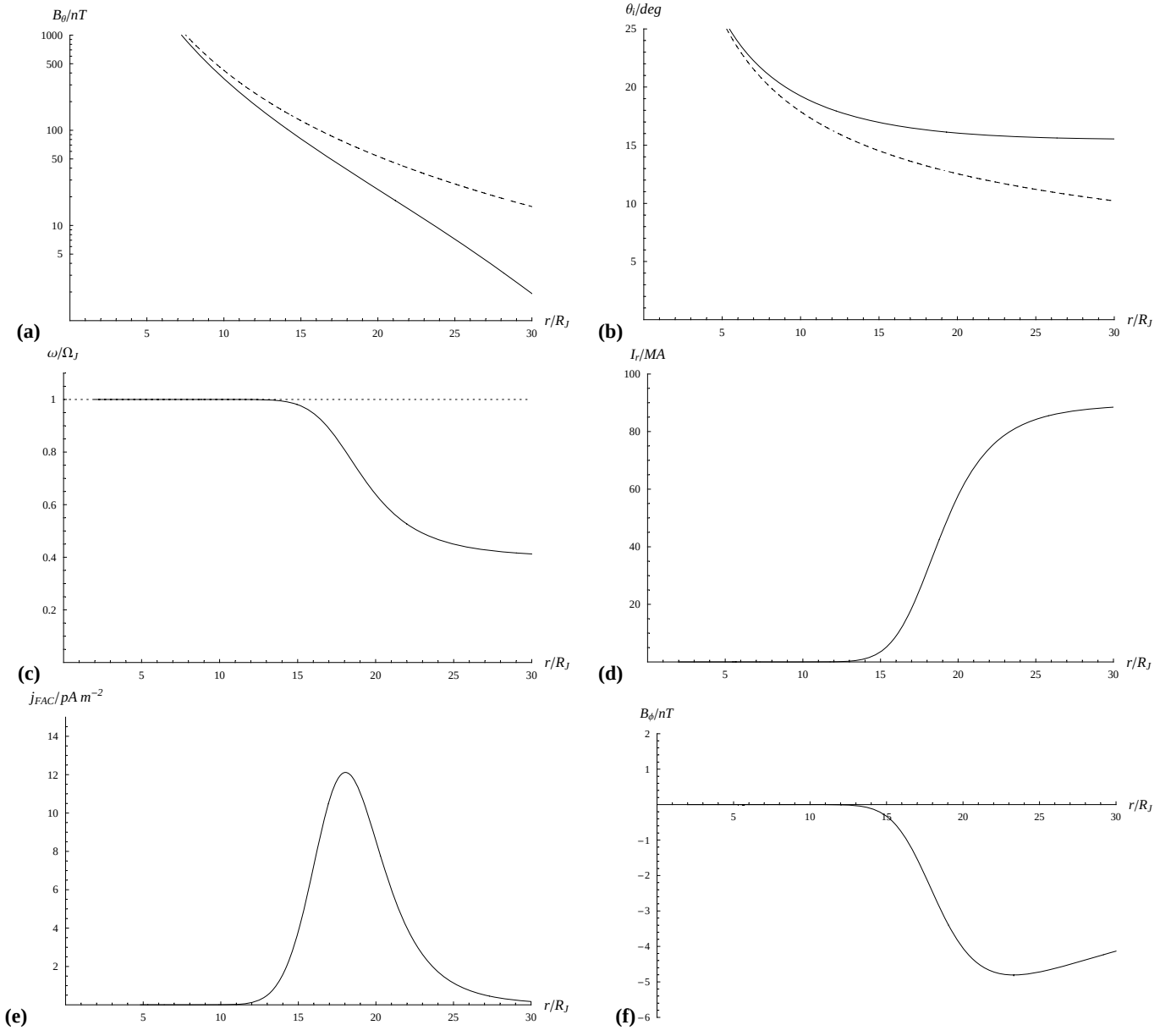

Fig. 3. Model parameters plotted versus radial distance in the equatorial plane for the steady-state model whose ionospheric profiles are shown in Figs. 1 and 2. The panels of the figure show **(a)** the magnetic field B_θ in the equatorial plane (positive southward), where the solid line shows the total model field including that of the equatorial current sheet, while the dashed line shows the inverse cube field of the planetary dipole alone, **(b)** the co-latitude θ_i of the field lines mapped from the equator to the ionosphere with respect to either pole, where the solid and dashed lines show the mapping for the total field and the planetary dipole field alone as in panel (a), **(c)** the angular velocity of the plasma normalised to the planetary angular velocity, where the dotted line corresponds to rigid corotation, **(d)** the azimuth-integrated radial current I_r flowing in the equatorial plane, equal to the sum of the azimuth-integrated Pedersen currents flowing in the conjugate northern and southern ionospheres (i.e. twice the current flowing in one hemisphere due to assumed north-south symmetry), **(e)** the field-aligned current density mapped from the ionosphere (Fig. 1c) to the equatorial plane using Eq. (8), and **(f)** the azimuthal field produced by the magnetosphere-ionosphere current system just north of the magnetic equator assuming for simplicity that the radial current shown in panel (d) flows in a thin sheet in the equatorial plane.

comparison. In the latter case the equatorial region out to 30 R_J extends poleward to an ionospheric co-latitude of $\sim$10.5°, thus encompassing almost the whole of the closed field region of the ionospheric model. With the inclusion of the current sheet, however, the mapping reaches only to $\sim$15.5° in the ionosphere, corresponding to a point within

the middle magnetosphere layer (the main upward current layer of which spans ∼15.3°–16.9°), located near its poleward border. As noted above, the parameters of the ionospheric model were adjusted slightly compared to Cowley et al. (2005) to ensure that this layer maps appropriately into the equatorial plane using the above field model.

Figure 3c then shows the normalised plasma angular velocity plotted versus radial distance in the equatorial plane, obtained from the value in the conjugate ionosphere (Fig. 1a), since as noted above in a steady state the angular velocity must be constant along each field line. The model plasma flow is then rigidly corotating (dotted horizontal line) in the inner magnetosphere, begins to decrease toward lower angular velocities at $\sim 15\,R_J$, and reaches ∼40% of rigid corotation at the outer boundary of the modelled region. The corresponding azimuth-integrated outward radial current within the equatorial current sheet I_r is shown in Fig. 3d, equal to twice the equatorward-directed Pedersen current in the conjugate ionosphere (Fig. 1b) due to the contributions from both hemispheres. Here we have assumed for simplicity that the field-aligned current flows from each ionosphere directly into the equatorial plane where it feeds a sheet of radial current whose azimuth-integrated value is shown in the figure. More realistically the radial current will flow in a distributed manner within the equatorial current sheet of half-width D, in which case the value shown is the total current flowing outward through the current sheet across the field line that maps to radius r in the equatorial plane. The value rises rapidly beyond $\sim 15\,R_J$ as expected from the angular velocity profile, and begins to plateau at ∼90 MA near the outer boundary of the region. This behaviour is intended to represent the equatorial radial current profile derived by Nichols and Cowley (2004) from the Galileo azimuthal magnetic field data presented by Khurana (2001), and helped motivate the choice of 0.25 mho for the effective ionospheric Pedersen conductivity.

The field-aligned current density flowing into the equatorial plane from both sides in the above thin equatorial radial current sheet approximation is shown versus radial distance in Fig. 3e, given by Eq. (8) with $B=B_\theta\,(r)$. Due to the large change in field strength along field lines between the ionosphere and equatorial plane in the relevant region, by factors of $\sim 10^4$–10^5, it can be seen that the field-aligned current density in the magnetosphere is much reduced compared with that in the ionosphere, peaking at $\sim 12\,\mathrm{pA\,m^{-2}}$ near $\sim 18\,R_J$. Thus while the upward field-aligned current in the ionosphere exceeds those that can be carried by the magnetospheric electron source populations by an order of magnitude or more, $\sim 100\,\mathrm{nA\,m^{-2}}$ by order of magnitude compared with $\sim 10\,\mathrm{nA\,m^{-2}}$ for the outer and middle magnetosphere source populations (see Table 1), hence requiring field-aligned electron acceleration, the reverse is true in the near-equatorial magnetosphere. Here the "current" associated with magnetospheric electrons moving in one direction along the field (i.e. the number flux of those electrons times the electron charge) remains the same as just given ($\sim 10\,\mathrm{nA\,m^{-2}}$), assuming a near-isotropic population, while the field-aligned current density $\sim 10\,\mathrm{pA\,m^{-2}}$ is less by three orders of magnitude. Thus the field-aligned current density in the magnetosphere is essentially impossible to measure directly from the associated anisotropies of the magnetospheric particle distributions, as indicated in Sect. 1. However, the presence of the magnetosphere-ionosphere coupling current system is readily observable from the azimuthal field it produces. This is shown versus radial distance in Fig. 3f for the region just northward of the equatorial plane, obtained from Eq. (9) using the same simple thin equatorial current sheet assumption as discussed above. The field is negative (i.e. "lagging") consistent with sub-corotation in the Northern Hemisphere, and rises in magnitude from small values in the inner magnetosphere to peak at ∼5 nT near to $\sim 23\,R_J$ before falling slowly again with increasing distance. The corresponding field south of the equator is, of course, just reversed in sign compared with that in the north. This profile is in good agreement with the Galileo results for the azimuthal field presented by Khurana (2001) (see also Nichols and Cowley, 2004). We note from Ampère's law that the azimuthal field just outside the equatorial radial current sheet is related to the total current I_r in the sheet (Fig. 3d) by $B_\varphi = \mp \mu_o I_r / 4\pi r$, where the upper and lower signs correspond to the region north and south of the equatorial plane respectively. Thus the B_φ profile is in agreement with the results of Khurana (2001) for the same reason that the I_r profile is also in good agreement as mentioned above (see Nichols and Cowley, 2004). In practice, of course, B_φ is the directly measured quantity, and I_r is derived from it via Ampère's law (Khurana, 2001; Nichols and Cowley, 2004).

Since the azimuthal field is a key diagnostic of the magnetosphere-ionosphere coupling current system, in Fig. 4a we show a contour plot of B_φ in a magnetic meridian plane, specifically for the region $0 \le \rho \le 30\,R_J$ and $-15 \le z \le 15\,R_J$, where ρ is the perpendicular distance from the magnetic axis as above and z is distance along the axis from the equatorial plane. The black dotted rectangle shows a cross-section through the equatorial current disk where the azimuthal current given by Eq. (16) flows in the model. The black solid lines show the magnetic field lines in the meridian, obtained by contouring the flux function. Specifically we show field lines that map to the ionosphere at co-latitudes θ_i of 5°–25° (with respect to both magnetic poles) at steps of 5°, thus spanning the region from the poles to the inner region of near-rigidly corotating field lines (see Fig. 1a). While the inner field lines are quasi-dipolar in form as expected, the higher-latitude field lines are strongly radially extended due to the azimuthal currents in the equatorial sheet. The green lines in the plot are also magnetic field lines, and delineate the field lines on which the major upward-directed field-aligned currents flow in the steady-state model. Specifically the outer pair of solid green lines in the upper and lower regions of the figure correspond to the north and south

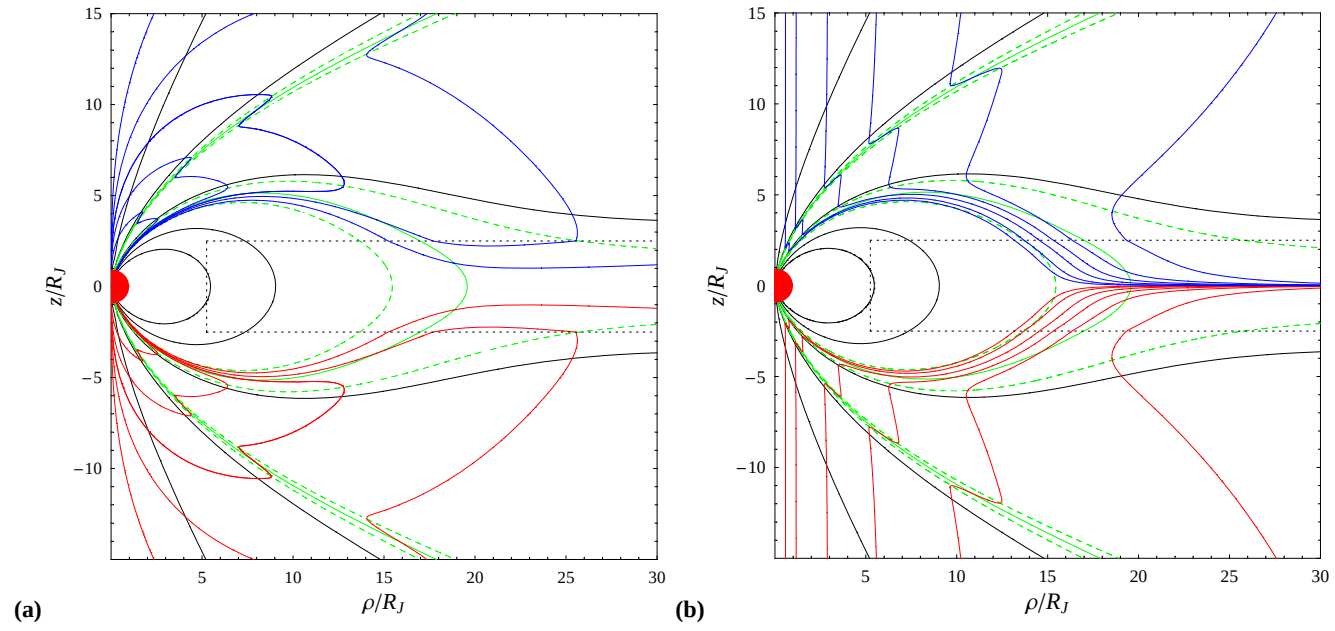

Fig. 4. Plots of fields and currents in the magnetic meridian plane for the steady-state model shown in Figs. 1–3, for the region $0 \le \rho \le 30\ R_J$ and $-15 \le z \le 15\ R_J$, where ρ is the perpendicular distance from the magnetic axis and z is the distance along the axis from the equatorial plane. The black solid lines in both panels show magnetic field lines mapping to the ionosphere at co-latitudes of 5°–25° relative to the northern and southern magnetic poles, at steps of 5°. The field is the sum of the planetary dipole and the field of the equatorial current sheet flowing within the black dotted rectangle. The green lines, also magnetic field lines, show the regions of upward-directed field-aligned current in the model, where the solid lines show the central field line of the current layer and the dashed lines the approximate boundaries on either side. Specifically, the current regions shown by the outer pair of green solid lines in the Northern and Southern Hemispheres map to the model open-closed field line boundaries at $\theta_i = \theta_{iO} = 10.716°$ with respect to both poles, while the corresponding green dashed lines map to $\theta_i = \theta_{iO} \pm 1.5\Delta\theta_{iO} = 10.716° \pm 0.1875°$ in both hemispheres. Similarly the green solid line in the equatorial region of the plots maps to the centre of the ionospheric "middle magnetosphere" layer at $\theta_i = \theta_{iMM} = 16.1°$, while the corresponding green dashed lines map to $\theta_i = \theta_{iMM} \pm 1.5\Delta\theta_{iMM} = 16.1° \pm 0.75°$. In panel (a) the red and blue solid lines show positive and negative contours, respectively, of the azimuthal field B_φ produced by the magnetosphere-ionosphere coupling current system, where from the outer to the inner contours shown, the field magnitudes are 2, 5, 10, 20, and 50 nT. In panel (b) the contours show the tilt angle of the field out of magnetic meridians produced by the azimuthal field, given by Eq. (18). From left to right the contours are for tilt angle magnitudes of 0.1°, 0.2°, 0.5°, 1°, 2°, and 5°.

open-closed field line boundaries, respectively, mapping to the ionosphere at $\theta_{iO} = 10.716°$ with respect to the poles, while the solid green line in the central region of the figure corresponds to the centre of the middle magnetosphere layer, mapping to the ionosphere at $\theta_{iMM} = 16.1°$. The dashed green lines on either side of the solid green lines then delineate the approximate width of the associated upward-directed current layers, given by the field lines mapping to the ionosphere at co-latitudes $\theta_{iO} \pm 1.5\Delta\theta_{iO} = 10.716° \pm 0.1875°$ and $\theta_{iMM} \pm 1.5\Delta\theta_{iMM} = 16.1° \pm 0.75°$, respectively. As expected from the results in Fig. 3, the upward field-aligned current in the ionospheric "middle magnetosphere layer" maps into the equatorial plane principally at radial distances beyond $\sim 15\ R_J$, centred near to $\sim 20\ R_J$, while the polar currents are confined to higher latitudes well away from the current sheet. The red and blue lines in the figure then show contours of constant B_φ produced by this current system, determined from Eq. (9), where the red lines in the Southern Hemisphere correspond to positive field values and the blue in the Northern Hemisphere to negative field values. From the outside to the inside, the nested contours plotted show B_φ field magnitudes of 2, 5, 10, 20, and 50 nT. In this plot we have also made a more realistic assumption that the radial cross-field current in the equatorial plane that closes the field-aligned current system flows in a distributed manner through the equatorial current disc. Specifically, we have assumed for simplicity that along each field line passing through the equatorial plane the azimuthal magnetic field within the current layer is given by Eq. (9) multiplied by the factor $f = |z| / D$, where z is again the distance from the magnetic equator. The azimuthal field then varies near-linearly across the width of the equatorial current layer, passing smoothly through zero in the magnetic equatorial plane itself (rather than undergoing a step-change at the equator as assumed for simplicity in Fig. 3). This feature aside, the azimuthal field contours in the plot essentially represent an extension into the

magnetosphere of the ionospheric azimuthal field shown in Fig. 1d, diminishing in magnitude with distance along each field line inversely with the perpendicular distance ρ from the magnetic axis (Eq. 9).

If we thus consider field lines in the vicinity of the open-closed field boundary and main oval, for which $\rho \approx 0.25\,R_J$ in the ionosphere, an azimuthal field of $\sim$500 nT in the ionosphere (Fig. 1d) drops to $\sim$10 nT at a distance of $\sim 10\,R_J$ from the axis, and $\sim$5 nT at a distance of $\sim 25\,R_J$, as can be seen in Fig. 4a. However, between these points the strength of the poloidal field in the dipole meridian plane falls by a much larger factor, the planetary field itself decreasing inversely as the cube of the distance at a given co-latitude. Consequently, although the field deflections produced by the azimuthal component are very small at ionospheric heights, peaking at $\sim 0.03^\circ$ as indicated above, they increase to much larger values at larger distances. We demonstrate this in Fig. 4b where we show a contour plot of the field tilt angle α_B, defined by

$$\tan\alpha_B = B_\varphi \big/ B_p, \tag{18}$$

where $B_p = \sqrt{B_r^2 + B_\theta^2}$ is the strength of the poloidal field. Angle α_B is thus the angle of the total field vector to the dipole meridian plane, with the sign the same as that of B_φ. In Fig. 4b positive and negative values are again shown by red and blue contours, respectively, while the magnitude of the tilt angle contours increases from left to right in the plot through values of 0.1°, 0.2°, 0.5°, 1°, 2°, and 5°. It can be seen that the tilt angle is typically a few degrees in the sub-corotating region of the magnetosphere, decreasing to a few tenths of a degree at distances within $\sim 3\,R_J$ of the planetary magnetic axis. In the latter regime the contours form piecewise quasi-straight line segments parallel to the z-axis. This follows from Eq. (9) combined with Eqs. (1), (2), and (6), from which it can be shown that in the high-latitude magnetosphere the field tilt angle is given approximately by

$$\tan\alpha_B \approx \mp\mu_o \Sigma_P^* \left(\Omega_J - \omega\right)\ \rho. \tag{19}$$

Thus in any such region where the plasma angular velocity is approximately constant, such as the open field region in our model and the outer magnetosphere region between the two layers of field-aligned current, the field tilt angle is nearly independent of z, and varies approximately linearly with perpendicular distance from the magnetic axis, depending on the degree of plasma sub-corotation.

4 Model for transient newly-compressed conditions

4.1 Flows and currents in the ionosphere

While the results discussed in Sect. 3 are expected to be representative of near-steady state conditions, singularly different behaviour is expected to be transiently produced during sudden major solar wind compressions of the magnetosphere. These may be associated with corotating interaction regions (CIRs) or coronal mass ejections, and can in some cases compress the system by a factor of two in linear dimension in a few hours (e.g. Nichols et al., 2006). Amongst the phenomena that may result from such compressions, a central physical effect anticipated is that of increasing the angular velocity of the plasma in the closed field region of the magnetosphere via conservation of angular momentum, potentially leading to transient super-corotation for major compressions and thus to a reversal in the sense of the middle magnetosphere coupling currents. This is the effect examined by Cowley et al. (2007) and modelled here, where for purposes of illustration we present results for an angular velocity model intended to represent conditions following a major compression from a subsolar magnetopause radius of $\sim 85\,R_J$ inwards to $\sim 45\,R_J$ (shown in Figs. 6 and 9 of Cowley et al., 2007). Such a magnetopause displacement would result e.g. from a sudden increase in the solar wind dynamic pressure from a rarefaction region value of $\sim$0.02 nPa to a CIR compression region value of $\sim$0.3 nPa across an interplanetary shock (Huddleston et al., 1998). We emphasise that such super-corotation conditions may prevail only for intervals of $\sim$6–12 h following such compressions before magnetosphere-ionosphere coupling and sub-corotation conditions re-assert themselves (Cowley et al., 2007). Nevertheless, the conditions during such intervals should be sufficiently different from the norm that they should be very evident in spacecraft data, such that it is worth brief exploration here.

To represent the above super-corotation conditions by a simple analytic function, we modify the constant value $\left(\omega_i \big/ \Omega_J\right)_{OM}$ in Eq. (15) to the function

$$\left(\frac{\omega_i\,(\theta_i)}{\Omega_J}\right)_{OM} = 0.5 + 4\sin\theta_i + 3.9\sin^{30}\theta_i \quad . \tag{20}$$

We also modify the parameters to the values θ_{iMM}=15.1° and $\Delta\theta_{iMM}$=0.6°. The resulting angular velocity profile is shown versus ionospheric co-latitude in Fig. 5a, which comparison shows contains the essential features of Fig. 6a of Cowley et al. (2007). The angular velocity is assumed to remain small on open field lines, but then increases rapidly to modestly super-corotating values on outer magnetosphere field lines adjacent to the magnetopause. The plasma then increasingly super-corotates deeper into the outer magnetosphere, peaking at $\left(\omega_i \big/ \Omega_J\right) \approx 2$ near the boundary between the outer and middle magnetosphere as predicted by the algorithm of Cowley et al. (2007), before falling to near-rigid corotation across the middle magnetosphere layer. We note, however, that by conservation of magnetic flux the open-closed field line boundary and the outer-middle magnetosphere regions do not change position in the ionosphere during such compressions.

The associated azimuth-integrated ionospheric horizontal Pedersen current is shown in Fig. 5b, where again positive

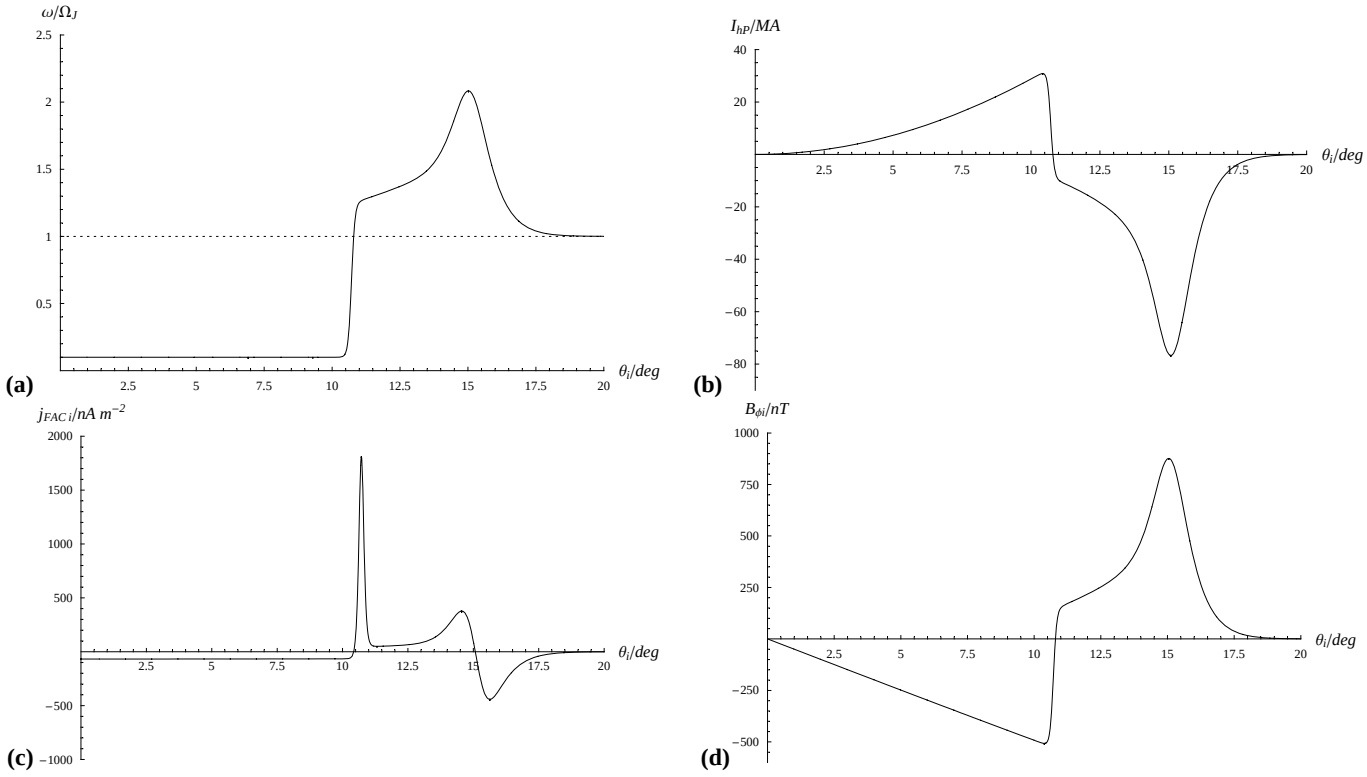

Fig. 5. Plasma flow and current system in the northern high-latitude ionosphere for the newly-compressed angular velocity model representing transient super-corotation conditions on outer and middle magnetosphere closed field lines produced by a major solar wind-induced compression of the magnetosphere, as given by Eqs. (15) and (20). The figure format is the same as for Fig. 1.

values indicate equatorward currents, and negative values poleward currents. In this case the equatorward current grows within the sub-corotating region of open field lines as before, but then reverses sense to poleward in the super-corotating region on closed field lines. The step in total current at the open-closed field line boundary is now ∼40 MA, significantly larger than in the quasi-steady case shown in Fig. 1, leading to much larger upward field-aligned current densities at this boundary. The poleward Pedersen current then increases to a negative maximum of ∼80 MA near the boundary between the outer and middle magnetosphere, before falling to small values across the middle magnetosphere as near-rigid corotation conditions are resumed in the inner region. The consequent field-aligned current densities are shown in Fig. 5c, where positive currents are again upward and negative currents downward, and where we also note the change in vertical scale compared with Fig. 1c. Here the upward current density at the open-closed field line boundary is increased to peak at $\sim 1.8\,\mu\mathrm{A\,m^{-2}}$ due to the enhanced flow shear across the boundary, while the sense of the current system on closed field lines is reversed compared with Fig. 1c, with upward currents on outer magnetosphere field lines peaking at $\sim 400\,\mathrm{nA\,m^{-2}}$ near the inner boundary, and similar downward currents on middle magnetosphere field lines in the adjacent equatorward region. The azimuthal field just above the ionosphere produced by this current system is shown in Fig. 5d. As in Fig. 1d, the azimuthal field is negative ("lagging") on sub-corotating open field lines, peaking at ∼500 nT near the open-closed field line boundary. However, unlike the steady-state case it then reverses to positive ("leading") values on super-corotating closed field lines. Peak positive values in the model are ∼900 nT near the boundary between the outer and middle magnetosphere, corresponding to a "leading" tilt of the field just above the ionosphere of ∼0.05°.

The corresponding auroral parameters associated with the upward current regions are shown in Fig. 6. Figure 6a again shows the field-aligned current density, now on an expanded co-latitude scale, while Fig. 6b shows the minimum field-aligned acceleration voltage. This voltage has now increased to ∼1 kV just poleward of the open-closed field line boundary where the current is carried by magnetosheath electrons, and to ∼50 kV just equatorward of the boundary where the current is carried by outer magnetosphere electrons. Lower accelerating voltages are then present throughout the upward current region in the outer magnetosphere, being relative low, ∼1–2 kV, in the outer part of the region, while increasing to ∼10 kV near its interface with the middle magnetosphere.

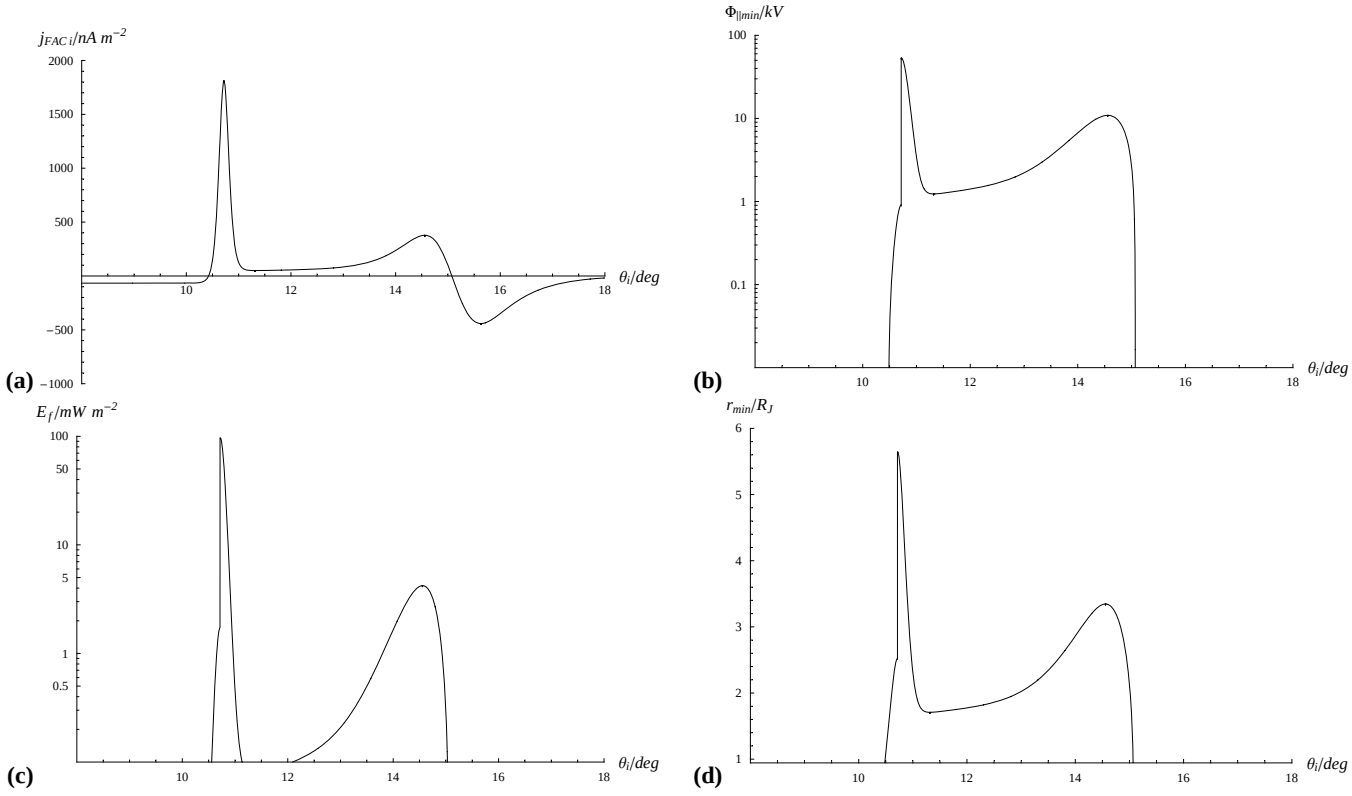

Fig. 6. Auroral acceleration parameters in the upward-directed field-aligned current regions shown in Fig. 5, representative of transient super-corotation conditions on outer and middle magnetosphere closed field lines produced by a major solar wind-induced compression of the magnetosphere. The figure format is the same as for Fig. 2.

We note that while the peak current densities in this region are comparable to those in the middle magnetosphere in the quasi-steady state model, the acceleration voltages required to produce these currents are lower than in the latter case because of the lower temperature of the outer magnetosphere source electrons in our model (Table 1). The corresponding precipitating electron energy fluxes shown in Fig. 6c then peak at $\sim$100 mW m^{-2} at the open-closed field line boundary, indicating the presence of a narrow very bright auroral arc with peak emission intensities of $\sim$1 MR. At lower latitudes a secondary broader region of enhanced precipitation is then formed in the outer magnetosphere region, mapping immediately poleward of the previous middle magnetosphere main oval in Fig. 2c, peaking at an energy flux of $\sim$4 mW m^{-2} corresponding to UV emission of $\sim$40 kR. Figure 6d then shows that the minimum radial distance of the auroral acceleration region must exceed $\sim 5\,R_J$ at the open-closed field line boundary where the current is carried by outer magnetosphere electrons. However, the acceleration region can be located closer to the planet in the more extended outer magnetosphere region of upward current at larger co-latitudes, above $\sim 3\,R_J$ near its inner edge where the upward current density peaks.

4.2 Flows and fields in the magnetosphere

In Fig. 7 we show corresponding model parameters versus radial distance in the equatorial plane in the same format as Fig. 3. Now, however, we modify the model magnetospheric magnetic field to reflect the compressed condition by adding a uniform southward-directed field of 9 nT to the steady-state model described above, representing in a simple way the additional near-planet internal field produced by the enhanced and inwardly-displaced magnetopause current system. The presence of this field then adds a third flux function term to the right-hand side of Eq. (17) given by $F_c = B_z\rho^2/2 = B_z r^2 \sin^2\theta/2$ with $B_z = -9$ nT. The magnitude of this field is in agreement with the previous discussion of such compression effects by Cowley et al. (2007) (see their Fig. 1b). The modified B_θ field in the equatorial plane is shown versus radial distance in Fig. 7a. This remains weaker than the planetary dipole field alone (dashed line) at all distances, but by a significantly smaller factor in the outer part of the system than for the steady-state model shown in Fig. 3a. Correspondingly, the field lines from a given position in the outer equatorial region now map closer to the pole than previously, as shown in Fig. 7b. In particular, the

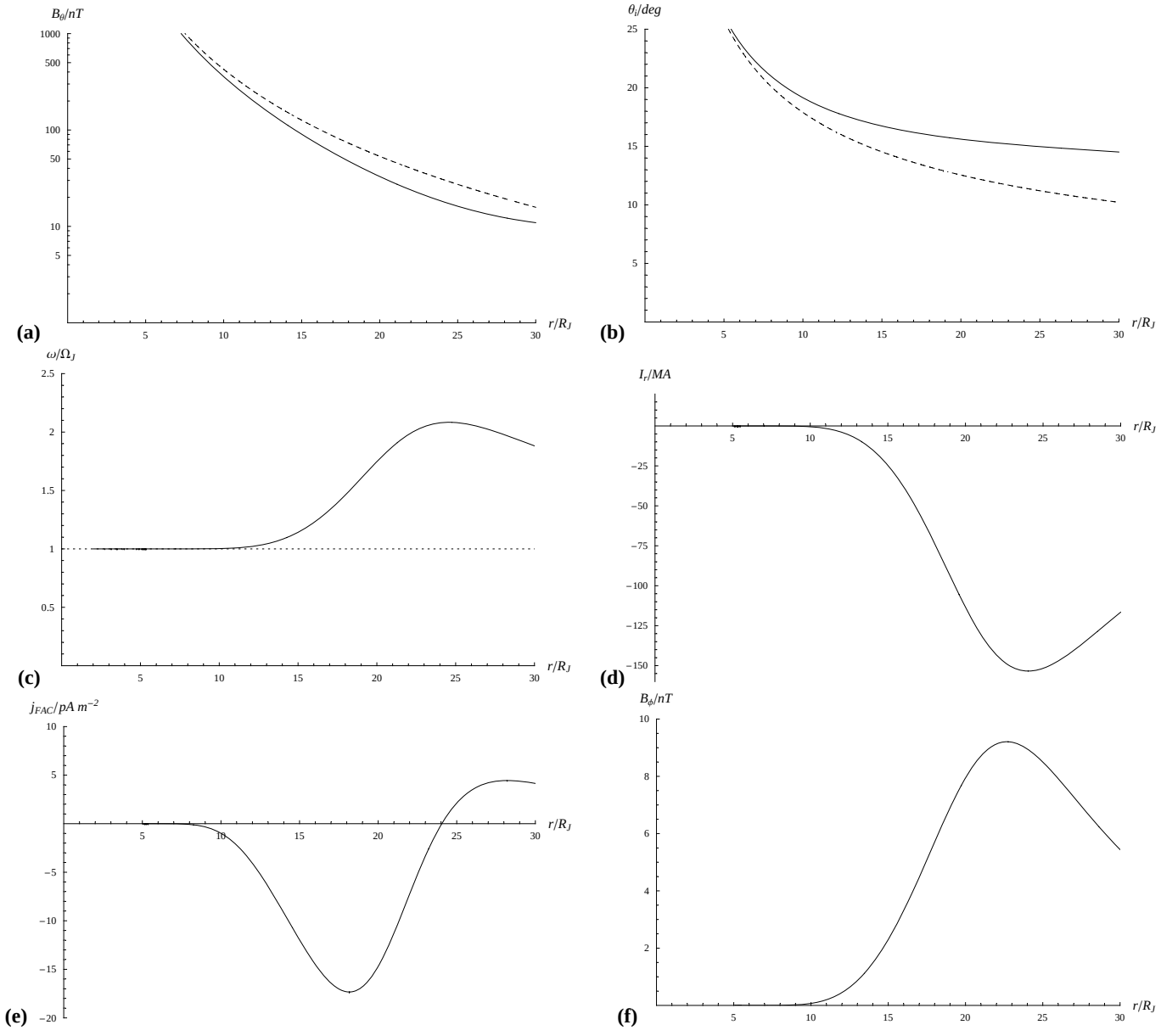

Fig. 7. Model parameters plotted versus radial distance in the equatorial plane for the newly-compressed magnetosphere model whose ionospheric profiles are shown in Figs. 5 and 6. The format of the figure is the same as for Fig. 3.

equatorial field line at the largest distance shown of 30 R_J now maps to ∼14.5° in the ionosphere compared to ∼15.5° in Fig. 3b. The radial variation of the plasma angular velocity mapped from the ionospheric profile in Fig. 6a is shown in Fig. 7c. The plasma now significantly super-corotates beyond ∼15 R_J, peaking at $\left(\omega/\Omega_J\right) \approx 2$ near ∼25 R_J, before slowly falling again at larger distances. As shown in Fig. 7d, the azimuth-integrated equatorial radial current I_r is correspondingly reversed in sense compared with quasi-steady conditions, now being directed radially inwards (negative) and peaking in magnitude at ∼150 MA near ∼24 R_J. The associated field-aligned current mapped to the equatorial plane shown in Fig. 7e is also reversed in sense, being directed inward to the planet (negative) in the inner region between ∼10 and ∼25 R_J, peaking in magnitude at ∼17 pA m^{-2} at ∼18 R_J, before reversing in sense to outward (positive) in the outer part of the region. The northern equatorial azimuthal field produced by these currents is similarly reversed in sense to positive as shown in Fig. 7f, thus corresponding to a "leading" field configuration, peaking at ∼9 nT near ∼22 R_J.

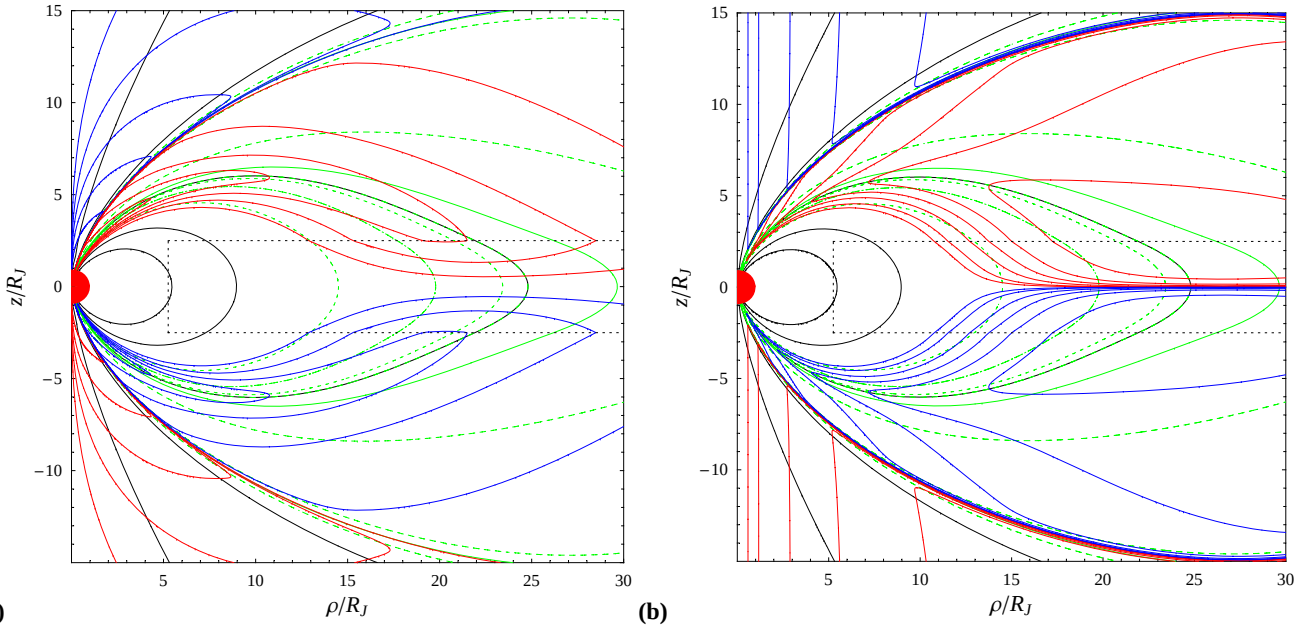

Fig. 8. Plot of fields and currents in the magnetic meridian plane for the newly-compressed magnetosphere model shown in Figs. 5–7. The format is the same as for Fig. 4, except for the green lines marking the field-aligned current systems in the central closed field region of the plot. Here the solid and dot-dashed green lines map to the peak in the closed-field upward- and downward-directed field-aligned currents in the ionosphere, respectively, as shown in Fig. 6a. The ionospheric co-latitudes are 14.55° for the upward current (solid green line) and 15.65° for the downward current (dot-dashed green line). The green dashed lines on either side of these lines then show where the peak current magnitudes ($\sim$400 nA m^{-2}) have fallen to 100 nA m^{-2}. The ionospheric co-latitudes are 13.25° and 15.00° for the upward current region, and 15.15° and 16.90° for the downward current region. Panel **(a)** shows B_φ contours, where the nested contours in each red (positive) and blue (negative) region again correspond to field magnitudes of 2, 5, 10, 20, and 50 nT from outside to inside in each case. Panel **(b)** similarly shows contours of the tilt angle of the field with respect to the magnetic meridian, where from left to right in each red (positive) and blue (negative) region the nested contours show tilt angle magnitudes of 0.1°, 0.2°, 0.5°, 1°, 2°, and 5° (the latter value does not occur in the open field region shown).

Plots of fields and currents in the dipole meridian plane for the newly-compressed model are shown in Fig. 8, in the same format as Fig. 4. The magnetic field lines shown by the black solid lines again map to 5°–25° in the ionosphere at steps of 5°. Comparison with Fig. 4 shows that the inner field lines dominated by the planetary field are not much affected in the modified model, while those in the outer region are significantly displaced inward by the added southward field representing the compressed state. The green field lines indicating the locations of the field-aligned current layers are again defined as in Fig. 4 for the outer pair of layers corresponding to the northern and southern open-closed field line boundaries, thus mapping in the ionosphere to θ_{iO}=10.716° with respect to each pole for the green solid lines, and to $\theta_{iO}\pm1.5\Delta\theta_{iO}$=10.716°±0.1875° for the adjacent green dashed lines. The green field lines representing the field-aligned current system in the central regions, however, are defined with respect to the modified pattern of ionospheric field-aligned currents shown in Fig. 6a. Specifically, the green solid line corresponds to the peak in the upward field-aligned current in the inner part of the outer magnetosphere region mapping to $\theta_i\approx$14.55° in the ionosphere, while the dot-dashed line corresponds to the peak in the downward field-aligned current region in the middle magnetosphere layer mapping to $\sim$15.65°. The pair of green dashed lines on either side of these lines then somewhat arbitrarily show where the magnitude of the ionospheric field-aligned current density drops to 100 nA m^{-2} from peak magnitudes of $\sim$400 nA m^{-2} in each case (see Fig. 6a), corresponding to co-latitudes of $\sim$13.25° and $\sim$15.0° for the region of upward current (the latter line then overlying the black solid line mapping to 15° co-latitude in the ionosphere), and to $\sim$15.15° and $\sim$16.9° for the region of downward current. These field-aligned current layers then define the region of strong azimuthal fields located between them shown by the red and blue solid contour lines in Fig. 8a, where the red (positive) lines in the northern closed field region and the blue (negative) lines in the southern closed-field region correspond to the "leading" field configuration associated with plasma super-corotation. Again, from the outside in, the nested contour levels correspond to azimuthal field magnitudes of 2, 5, 10, 20, and 50 nT. Across the field-aligned

current layer mapping to the open-closed boundary, however, sub-corotation is resumed on open field lines in the model, leading to "lagging" fields of opposite polarity which are in essence similar to those shown in Fig. 4a. The field tilt angle contours in Fig. 8b show corresponding features. As in Fig. 4b, from left to right the contours shown in each nested region correspond to tilt angle magnitudes of 0.1°, 0.2°, 0.5°, 1°, 2°, and 5°, though the latter value does not occur in the open field region shown. The field tilts are again typically a few degrees within the closed field region of the magnetosphere, though now of opposite polarity to those for the quasi-steady state case in Fig. 4b, falling to a few tenths of a degree within a few planetary radii of the magnetic axis.

5 Steady-state model evaluation on the polar Juno orbit

In this section we show how the above models, defined with respect to the magnetic axis, may be evaluated in space and time e.g. along a spacecraft trajectory, taking account of the rotation of the magnetic axis around the planet's spin axis. Because of the transient nature of the newly-compressed conditions discussed in Sect. 4, however, here we will illustrate our results only for the steady state model of Sect. 3. Specifically, we will employ the planning trajectories of the forthcoming NASA New Frontiers Juno mission, which will be the first spacecraft to obtain true polar observations in Jupiter's magnetosphere, including plasma and field data together with remote sensing observations of UV emissions in the conjugate ionosphere (http://juno.wisc.edu/). Juno is due for launch in August 2011, and after Jupiter orbit insertion manoeuvres in late 2016, the spacecraft will acquire data on thirty-one 11-day science orbits between November 2016 and December 2017, before de-orbit takes place at the end of the mission. The orbit is planned as very closely polar relative to the planet's spin axis throughout, with apoapsis at 39 R_J and periapsis at 1.06 R_J, these values also remaining almost constant over the mission. Initially, the line of apsides of the orbit will be close to equatorial, with apoapsis located at ∼5° latitude in the Southern Hemisphere (at a local time (LT) of ∼05:30 h in the dawn sector). However, due to the oblateness of the planet, the line of apsides will rotate significantly during the course of the mission, with apoapsis reaching a latitude of ∼35° in the Southern Hemisphere (at 04:30 LT) by the mission end.

Given this orbit together with the axi-symmetry of the model about the magnetic axis, the principal orbit variables to be considered are the inclination of the line of apsides relative to Jupiter's spin equator, taken here for simplicity to be constant on each orbit, together with the phasing of the spacecraft position in its orbit relative to the rotation of the magnetic dipole axis around the planet's spin axis. As noted in the introduction, according to the VIP4 model the dipole axis is tilted through an angle of θ'_D=9.515° relative to the spin axis. For simplicity we define the zero of azimuth φ' around the planet's spin axis as the meridian plane that contains the periapsis pass of the spacecraft, the remainder of the polar orbit (centred at apoapsis) then being contained in the plane φ'=180°. Newton's laws then determine the orbit of the spacecraft as radial distance $r_S\,(t)$ and co-latitude $\theta'_S\,(t)$ relative to the spin axis in the φ'_S=0°−180° plane versus time, for a given inclination of the line of apsides. For simplicity we also take the zero of time t to coincide with the periapsis time on each orbit. The azimuth of the tilted dipole axis around the spin axis (specifically for the northern pole) is then taken to be given by

$$\varphi'_D\,(t) = \Omega_J t + \varphi'_{D0} \quad , \tag{21}$$

where Ω_J is again the angular frequency of planetary rotation corresponding to a period of ∼9.93 h, and φ'_{D0} is the azimuth of the dipole axis relative to periapsis at the time of periapsis. Thus, for example, φ'_{D0}=0° corresponds the case in which the dipole axis lies in the orbit meridian plane at the time of periapsis, with the northern pole tilted toward the periapsis point. From geometry the co-latitude of the spacecraft relative to the magnetic axis at any time, $\theta\,(t)$, is then given by

$$\cos\theta\,(t) = \cos\theta'_D \cos\theta'_S\,(t) \pm \sin\theta'_D \cos\varphi'_D\,(t) \sin\theta'_S\,(t)\,, \tag{22}$$

where $\varphi'_D\,(t)$ is given by Eq. (21), and the upper sign corresponds to the periapsis orbit segment where φ'_S=0° while the lower sign corresponds to the apoapsis orbit segment where φ'_S=180°. This, combined with the radial distance of the spacecraft, then determines the spacecraft's magnetic mapping to the ionosphere in the model through Eq. (17), and hence the instantaneous values of the model parameters at the spacecraft.

Clearly the nature of the observations will be determined principally by the trajectory of the spacecraft relative to the magnetospheric structures, so we begin our discussion in Fig. 9 by plotting the spacecraft orbit in the magnetic meridian plane for three phases of the mission. Figure 9a corresponds to the early phase of the mission when the line of apsides is tilted by 5° relative to the equator, with apoapsis in the Southern Hemisphere. The trajectory is shown by the red solid line, which oscillates with the planetary period due to the rotation of the tilted magnetic dipole axis with the planet. For definiteness we have taken φ'_{D0}=90° in Eq. (21), a value that for simplicity is used for all the results presented here. This parameter determines the exact phase of the trajectory oscillations relative to the magnetic structures, but examination of a wide range of cases shows that the overall nature of the results is not strongly affected. Periapsis (i.e. t=0) on the trajectory is marked by the blue dot close to the planet, with subsequent blue dots being placed along the trajectory at 10 h intervals, the inbound pass being located principally north of the equator, and the outbound pass south of the equator. It can thus be seen that the plot encompasses a period of approximately ∼60 h (i.e. ∼2.5 days) on either

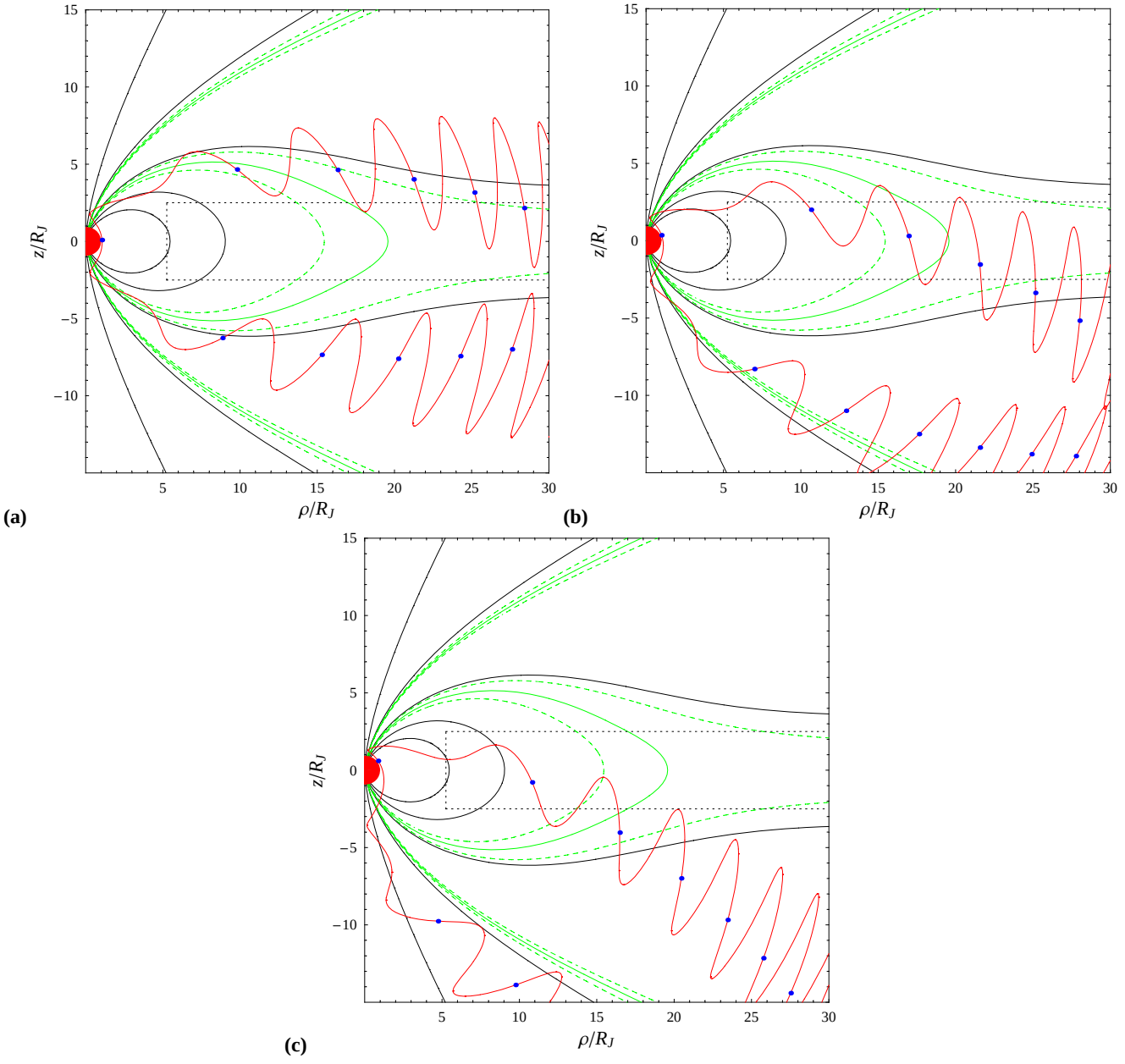

Fig. 9. Plots of the Juno trajectory (red solid line) in the magnetic meridian plane for three different phases of the mission. Panel **(a)** corresponds to the early mission phase when the line of apsides is inclined at 5° to the spin equator, with apoapsis in the Southern Hemisphere, panel **(b)** to the middle mission phase when the inclination of the line of apsides has increased to 20°, and panel **(c)** to the end of the mission when the inclination has increased to 35°. In each case we have chosen dipole phase φ'_{D0}=90° in Eq. (21). The blue dot on each trajectory close to the planet marks periapsis (time t=0), while the other blue dots mark intervals of 10 h on either side. The black and green lines show magnetic field lines and field-aligned current regions corresponding to the steady-state case as in Fig. 4.

side of periapsis. The 10 h interval has been chosen to allow ready comparison with the parameter plots to be shown in Figs. 10 and 11. It is also, of course, approximately the rotation period of Jupiter. The black and green lines in the plot show the magnetic field lines and field-aligned current regions for the steady-state model, as in Fig. 4. It can be seen that during the inbound pass the spacecraft position oscillates between the northern middle magnetosphere region mapping to the main oval and the northern outer magnetosphere region that overlays it, where the field lines close through the equator beyond the edge of the plot. On the outbound pass the spacecraft is located at somewhat higher latitudes due to

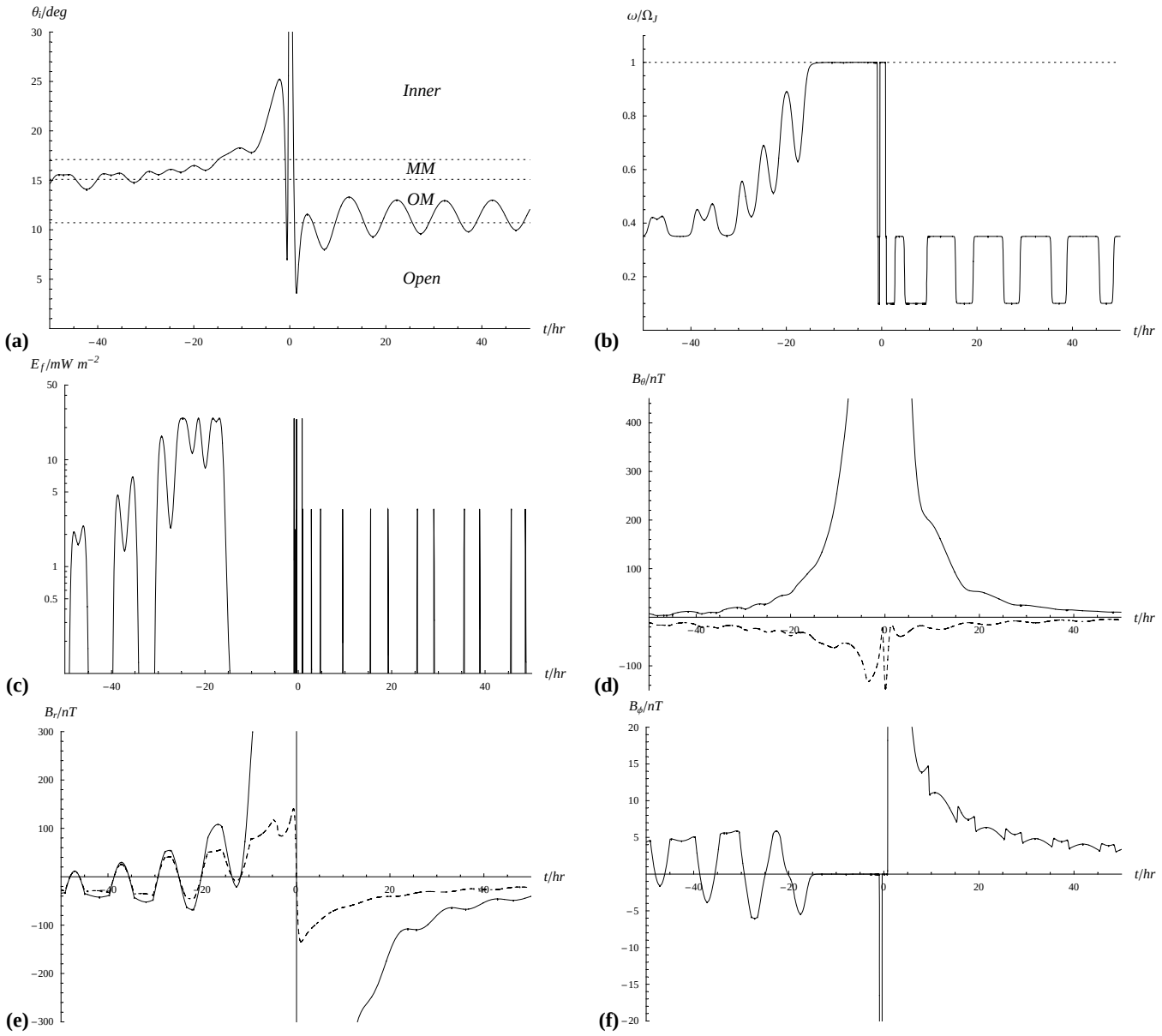

Fig. 10. Plots of plasma and field parameters versus time for the steady-state model and the middle-mission Juno orbit shown in Fig. 9b, with the line of apsides tilted by 20° and φ'_{D0}=90° in Eq. (21). The interval shown is ±50 h about periapsis. Panel **(a)** shows the co-latitude of the spacecraft mapped along field lines to the ionosphere, with respect to either pole. The horizontal dotted lines indicate the boundaries between the various regions of the model as defined by the plasma angular velocity profile, namely the open-closed field line boundary at 10.716° which marks the boundary between "Open" and closed outer magnetosphere ("OM") field lines, the boundary between the latter region and the middle magnetosphere ("MM") at 15.1°, and the boundary between the middle and "Inner" magnetosphere at 17.1°. Panels **(b)** and **(c)** then show the normalised plasma angular velocity at the spacecraft, and the precipitating energy flux of accelerated auroral electrons at the feet of the field lines, respectively. Panels **(d–e)** show the three components of the magnetic field in spherical polar coordinates referenced to the magnetic axis, the azimuthal component being that produced by the magnetosphere-ionosphere coupling current system. In the panels showing the poloidal field components the solid line shows the total field component, while the dashed line shows the field of the equatorial current sheet alone.

the modest inclination of the line of apsides, and is mainly confined to the southern outer magnetosphere region beyond radial distances of ∼15 R_J. During the periapsis pass, however, the spacecraft penetrates at low altitude into the region of open field lines in both hemispheres, thus passing twice in each hemisphere across the regions of upward-directed

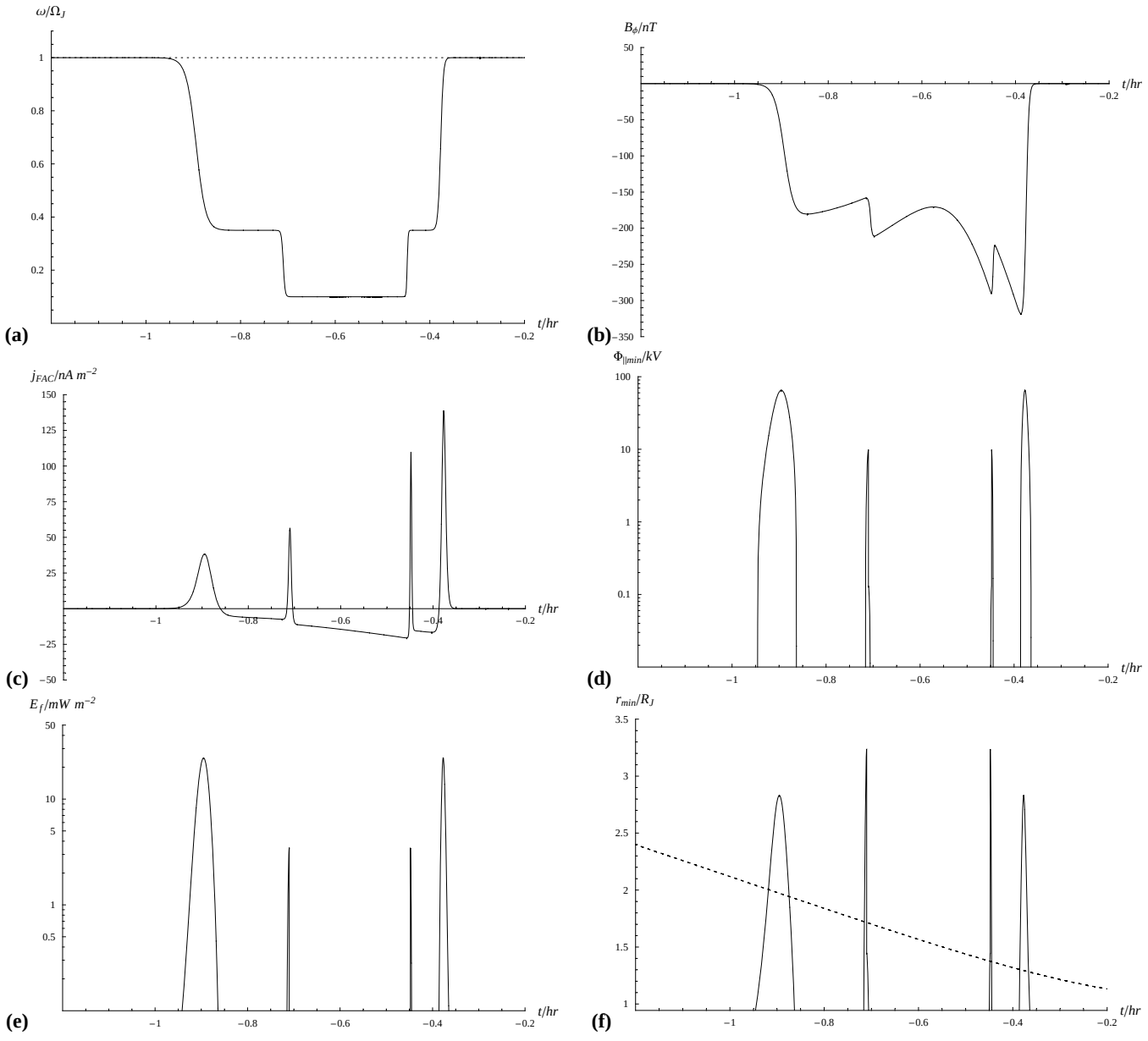

Fig. 11. Polar pass plots of parameters related to the magnetosphere-ionosphere coupling current system for the steady-state model and the middle-mission Juno orbit shown in Fig. 9b, with the line of apsides tilted by 20° and with φ'_{D0}=90° in Eq. (21). The interval shown corresponds to the pre-periapsis north polar pass between t=−1.2 h and −0.2 h (i.e. one hour in total). The panels of the figure show **(a)** the normalised plasma angular velocity, **(b)** the azimuthal field produced by the magnetosphere-ionosphere coupling current system, **(c)** the local field-aligned current density at the spacecraft where positive and negative values indicate upward- and downward-directed currents, respectively, **(d)** the minimum field-aligned accelerating voltage required by the field-aligned current density at the ionosphere, **(e)** the corresponding precipitating electron energy flux, and **(f)** the minimum radial distance of the auroral electron acceleration region. The dotted line in panel (f) also shows the radial distance of the spacecraft during the pass.

field-aligned current mapping to the main oval and the open-closed field line boundary.

Figure 9b similarly corresponds to the central part of the mission when the line of apsides is inclined at 20° to the equator. On the inbound pass the spacecraft now passes obliquely through the equatorial magnetosphere from south to north in the vicinity of ∼20 R_J, thus traversing the field lines of the middle magnetosphere layer from poleward to equatorward, while on the outbound pass it oscillates between open and outer magnetosphere field lines in the

Southern Hemisphere. Figure 9c then corresponds to near the end of the mission when the line of apsides is further inclined at 35° to the equatorial plane. Here on the inbound pass the spacecraft is initially located on southern outer magnetosphere field lines, crosses the middle magnetosphere and upward current region corresponding to the main oval at a radial distance of $\sim$15 R_J in the Southern Hemisphere, and then moves to periapsis through the central inner magnetosphere traversing the Io torus centred in the equatorial plane near $\sim$6 R_J. The outbound pass is confined to the region of open field lines within the portion of the orbit shown.

We now exemplify the results of our model by showing model parameters versus time along the Juno trajectory shown in Fig. 9b, corresponding to the middle mission interval when the line of apsides has a 20° tilt. In the initial sequence of plots in Fig. 10 we show results for an interval of $\pm$50 h about periapsis, thus characterising the overall inbound and outbound passes, while in Fig. 11 we examine the north polar pass at higher resolution. The key model parameter that determines the field and plasma conditions on the orbit is the co-latitude of the ionospheric mapping of the spacecraft footprint relative to either pole, shown in Fig. 10a using Eq. (17). The horizontal dotted lines in this figure delimit the principal regions of the model defined with respect to the behaviour of the plasma angular velocity, namely the open field region with a boundary (the open-closed boundary) at 10.716°, the outer magnetosphere ("OM") with an inner boundary mapping to the ionosphere at $\sim$15.1°, and the middle magnetosphere ("MM") layer with inner boundary mapping to $\sim$17.1°, inside of which the plasma near-rigidly corotates in the "inner" region. In conformity with Fig. 9b it can be seen, for example, that the spacecraft is magnetically connected to the upward current region mapping to the middle magnetosphere and main oval for many hours during the inbound pass ($t \leq 0$), makes two rapid passes across this region just pre-periapsis corresponding to the low-altitude north polar pass to be shown in Fig. 11, and then passes once across it at low altitude during the south polar pass post-periapsis. On the outbound pass the spacecraft then oscillates between the outer magnetosphere and open field lines. This mapping then determines the model parameters at the feet of the field lines, and hence those present at the spacecraft, exemplified in Fig. 10b and c. The normalised plasma angular velocity at the spacecraft is shown in Fig. 10b, which oscillates between outer and middle magnetosphere values on the inbound pass before ramping up towards rigid corotation as the spacecraft passes into the inner region, while cycling between outer magnetosphere and open field line values on the outbound pass. In Fig. 10c we plot the precipitating energy flux at the feet of the field lines, showing relatively extended intervals of connection to the main oval on the inbound pass, and repeated passes across the polar arc at the southern open-closed field line boundary on the outbound pass. In Fig. 10d–e we then show the three components of the model magnetic field at the spacecraft in spherical polar coordinates referenced to the magnetic axis. In the panels showing the poloidal field components the solid line shows the total field, while the dashed line shows the field of the equatorial current sheet alone. The planetary field dominates within $\pm$20 h about periapsis, corresponding to radial distances inside $\sim$15 R_J from the planet (Fig. 9b), while the current sheet field dominates outside this interval, giving rise to the strong periodic reversals in the radial field in the initial inbound interval due to crossings through the current sheet. These are absent on the outbound pass since the spacecraft is then confined to higher southern latitudes, but the field is still significantly radially distended by the current sheet. The azimuthal field in Fig. 10c then shows anti-phase variations with the radial field during the early inbound pass, corresponding to current sheet traversals of a "lagging" field configuration, with peak field deflections of $\sim$7.5° out of the magnetic meridian in either direction. As in Fig. 4 we have assumed that B_φ varies as $|z|/D$ along each field line within the equatorial current sheet region. The azimuthal field then falls to small values within the inner near-rigid corotation region. On the outbound pass the azimuthal field is consistently positive, corresponding to a lagging field and sub-corotational flow in the Southern Hemisphere, and shows considerable small-scale structure as the spacecraft cycles between the open field region and the outer magnetosphere, while overall falling relatively slowly with distance from the planet. Due to the much more rapid fall of the poloidal field, however, the field tilt angle grows steadily with time, from small values near periapsis to $\sim$5° in the later outbound pass (see Fig. 4b).

In Fig. 11 we focus at higher time resolution on the periapsis pass, specifically on the Northern Hemisphere pre-periapsis interval in which the spacecraft passes inbound from the northern inner near-rigid corotation region on one side of the planet, located near the dawn meridian on the Juno mission, across the field-aligned current structures to reach open field lines at highest magnetic latitudes, and then re-crosses these regions on the other side of the planet near dusk as the spacecraft approaches periapsis near the equator. The plots in the figure thus correspond to a one-hour interval, starting and ending 1.2 h and 0.2 h before periapsis, respectively. In Fig. 11a–c we show the normalised plasma angular velocity, the azimuthal field produced by the coupling current system, and the related current density at the spacecraft, while in Fig. 11d–f we show the corresponding auroral parameters, namely the minimum auroral acceleration voltage, the precipitating electron energy flux, and the minimum height of the electron acceleration region. The connection of the parameter variations to the ionospheric plots in Figs. 1 and 2 is now generally clear and does not require elaboration, the plots serving initially to show the time scales over which the main oval and polar arc field-aligned currents and precipitating particles will be crossed in situ on the trajectory, together with the corresponding changes in the plasma angular velocity and azimuthal field. For the main oval currents the

times scales are ∼3 min and ∼1 min for the dawn and dusk passes, respectively, while for the polar arc these times are reduced to ∼10 s. The corresponding changes in the azimuthal field are ∼200–300 nT across the main oval, and ∼50 nT across the polar arc. However, the overall deflection of the field out of magnetic meridians produced by the coupling currents is very small, typically in the range ∼0.05°–0.1°. The dashed line in Fig. 11f also plots the jovicentric radial distance of the spacecraft versus time so that it may be compared with the minimum height of the auroral field-aligned acceleration regions associated with the upward field-aligned currents. It can be seen that in all four traversals of the upward current regions, the spacecraft will pass underneath the acceleration regions at least in the centre of the current layer, and will thus observe the auroral primary electrons that result in the main oval and polar emissions. According to our acceleration model these will have peak energies of ∼65 kV for the main oval and ∼10 kV for the polar arc corresponding to the acceleration voltage shown in Fig. 11d, with energy fluxes sufficient to produce UV emissions of ∼250 kR and ∼30 kR, respectively, at the field line feet, as indicated in Fig. 11e.

6 Summary and conclusions

In this paper we have constructed two related magnetosphere-ionosphere coupling current models for the jovian system that directly connect current systems and related auroral emissions at the ionospheric level with field and flow effects in the magnetosphere beyond. The first of these is developed from the magnetosphere-ionosphere coupling model of Cowley et al. (2005), intended to represent quasi-steady sub-corotating states within the jovian system. The second is based on results derived by Cowley et al. (2007) describing the transient conditions produced by a sudden major compression of the magnetosphere due e.g. to a CIR event, in which plasma super-corotation is induced in the outer and middle regions. The principal assumption of these models is that of axi-symmetry about the magnetic axis, thus confining the region of approximate validity to the central part of the magnetosphere where effects associated with finite radial information propagation and solar wind-related asymmetries are unimportant. The models are formulated in terms of a plasma angular velocity profile versus magnetic co-latitude in the ionosphere, from which the ionospheric currents and auroral acceleration parameters can be calculated using appropriate ionospheric and magnetospheric plasma parameters. We then combine this model defined at ionospheric heights with a magnetospheric magnetic model consisting of a tilted rotating planetary dipole field and the field of a similarly tilted equatorial current sheet extending outward from the Io torus, to produce a corresponding axi-symmetric model of the flow, field, and currents in the magnetosphere that is taken to be valid within radial distances of ∼30 R_J from the planet.

The key feature of the combined model is thus that it allows a direct connection to be made between in situ observations in the magnetosphere, most specifically the plasma angular velocity and the azimuthal magnetic field produced by the magnetosphere-ionosphere coupling current system, and the auroral response in the ionosphere. This is a central experimental goal of the forthcoming NASA New Frontiers Juno mission, which will make the first observations at Jupiter from a polar orbit. Our extended model has therefore been evaluated along Juno planning orbits, with results illustrated here for our "steady state" model on a typical mid-mission orbit in which the line of apsides is inclined at ∼20° to Jupiter's equatorial plane. For such an orbit the spacecraft passes centrally through the current-carrying regions in the equatorial magnetosphere on its inbound pass, then over both northern and southern auroral regions at low altitudes near periapsis, before exploring open and outer magnetosphere field lines on the outbound pass at mid-latitudes. The model shows, for example, that while the spacecraft remains magnetically connected to the main oval over intervals of many hours within the middle magnetosphere region on the inbound pass, the low-altitude main oval over-passes near periapsis take place on time scales of ∼1–3 min. Polar arc traversal times scales on these passes are estimated to be of order ∼10 s. In all cases the polar passes occur underneath the corresponding auroral acceleration regions (which also holds true for the transient "compressed" model), the latter being predicted to form on auroral field lines typically at radial distances beyond ∼3 R_J. It is thus anticipated that the spacecraft particle instrumentation will indeed sample the accelerated auroral primaries during the periapsis passes, with typical electron energies of ∼50–100 keV for the main oval, and ∼10 keV for the polar arcs. The "lagging" angular field deflections from magnetic meridians produced by the associated magnetosphere-ionosphere current systems are also predicted to be of order ∼0.05°–0.15° on these passes, associated with azimuthal fields above the ionosphere of a few hundred nT. However, because the planetary field falls as the inverse cube of the distance from the planet, while the azimuthal field falls only inversely with distance from the magnetic axis on a given field line, the relative importance of the azimuthal field increases with distance from the planet, reaching ∼5°–10° in the middle and outer magnetosphere.

Acknowledgements. We thank Steven Levin and Stuart Stephens of the JPL Juno team for information on the Juno planning trajectory. AJD was supported by a University of Leicester SURE award, SWHC by STFC grant PP/D002117/1 and a Royal Society Leverhulme Trust Senior Research Fellowship, and EJB by STFC grant PP/E000983/1.

Topical Editor I. A. Daglis thanks J. Woch, P. Louarn, and another anonymous referee for their help in evaluating this paper.

References

Acuña, M. H., Behannon, K. W., and Connerney, J. E. P.: Jupiter's magnetic field and magnetosphere, in: Physics of the Jovian Magnetosphere, edited by: Dessler, A. J., Cambridge Univ. Press, Cambridge, UK, p. 1–50, 1983.

Barbosa, D. D., Scarf, F. L., Kurth, W. S., and Gurnett, D. A.: Broadband electrostatic noise and field-aligned currents in Jupiter's middle magnetosphere, J. Geophys. Res., 86, 8457–8369, 1981.

Bunce, E. J., Cowley, S. W. H., and Yeoman, T. K.: Jovian cusp processes: Implications for the polar aurora, J. Geophys. Res., 109, A09S13, doi:10.1029/2003JA010280, 2004.

Clarke, J. T., Ballester, G., Trauger, J., Ajello, J., Pryor, W., Tobiska, K., Connerney, J. E. P., Gladstone, G. R., Waite Jr., J. H., Ben Jaffel, L., and Gérard, J.-C.: Hubble Space Telescope imaging of Jupiter's UV aurora during the Galileo orbiter mission, J. Geophys. Res., 103, 20217–20236, 1998.

Clarke, J. T., Ajello, J., Ballester, G., Jaffel, L. B., Connerney, J., Gérard, J.-C., Gladstone, G. R., Grodent, D., Pryor, W., Trauger, J., and Waite, J. H.: Ultraviolet auroral emissions from the magnetic footprints of Io, Ganymede, and Europa on Jupiter, Nature, 415, 997–1000, 2002.

Clarke, J. T., Grodent, D., Cowley, S. W. H., Bunce, E. J., Zarka, P., Connerney, J. E. P., and Satoh, T.: Jupiter's auroras, in: Jupiter, edited by: Bagenal, F., Dowling, T. E., and McKinnon, W. B., Cambridge Univ. Press, Cambridge, UK, p. 639–670, 2004.

Clarke, J. T., Nichols, J. D., Gérard, J.-C., Grodent, D., Hansen, K. C., Kurth, W. R., Gladstone, G. R., Duval, J., Wannawichian, S., Bunce, E. J., Cowley, S. W. H., Crary, F. J., Dougherty, M. K., Lamy, L., Mitchell, D., Pryor, W., Retherford, K., Stallard, T. S., and Zieger, B.: The response of Jupiter's and Saturn's auroral activity to the solar wind, J. Geophys. Res., in review, doi:10.1029/2008JA013694, 2008.

Connerney, J. E. P., Acuña, M. H., and Ness, N. F.: Modeling the jovian current sheet and inner magnetosphere, J. Geophys. Res., 86, 8370–8384, 1981.

Connerney, J. E. P., Acuña, M. H., Ness, N. F., and Satoh, T.: New models of Jupiter's magnetic field constrained by the Io flux tube footprint, J. Geophys. Res., 103, 11929–11940, 1998.

Cowley, S. W. H. and Bunce, E. J.: Origin of the main auroral oval in Jupiter's coupled magnetosphere-ionosphere system, Planet. Space Sci., 49, 1067–1088, 2001.

Cowley, S. W. H. and Bunce, E. J.: Modulation of Jupiter's main auroral oval emissions by solar wind-induced expansions and compressions of the magnetosphere, Planet. Space Sci., 51, 57–79, 2003a.

Cowley, S. W. H. and Bunce, E. J.: Modulation of jovian middle magnetosphere currents and auroral precipitation by solar wind-induced compressions and expansions of the magnetosphere: Initial conditions and steady state, Planet. Space Sci., 51, 31–56, 2003b.

Cowley, S. W. H., Nichols, J. D., and Bunce, E. J.: Distributions of current and auroral precipitation in Jupiter's middle magnetosphere computed from steady-state Hill-Pontius angular velocity profiles: Solutions for current sheet and dipole magnetic field models, Planet. Space Sci., 50, 717–734, 2002.

Cowley, S. W. H., Bunce, E. J., Stallard, T. S., and Miller, S.: Jupiter's polar ionospheric flows: theoretical interpretation, Geophys. Res. Lett., 30(5), 1220, doi:10.1029/2002GL016030, 2003.

Cowley, S. W. H., Alexeev, I. I., Belenkaya, E. S., Bunce, E. J., Cottis, C. E., Kalegaev, V. V., Nichols, J. D., Prangé, R., and Wilson, F. J.: A simple axi-symmetric model of magnetosphere-ionosphere coupling currents in Jupiter's polar ionosphere, J. Geophys. Res., 110, A11209, doi:10.1029/2005JA011237, 2005.

Cowley, S. W. H., Nichols, J. D., and Andrews, D. J.: Modulation of Jupiter's plasma flow, polar currents, and auroral precipitation by solar wind-induced compressions and expansions of the magnetosphere: A simple theoretical model, Ann. Geophys., 25, 1433–1463, 2007, http://www.ann-geophys.net/25/1433/2007/.

Dessler, A. J. (Ed.): Physics of the Jovian Magnetosphere, Cambridge University Press, Cambridge, UK, 1983.

Edwards, T. M., Bunce, E. J., and Cowley, S. W. H.: A note on the vector potential of Connerney et al.'s model of the equatorial current sheet in Jupiter's magnetosphere, Planet. Space Sci., 49, 1115–1123, 2001.

Frank, L. A., Paterson, W. R., and Khurana, K. K.: Observations of thermal plasmas in Jupiter's magnetotail, J. Geophys. Res., 107(A1), 1003, doi:10.1029/2001JA000077, 2002.

Grodent, D., Clarke, J. T., Kim, J., Waite Jr., J. H., and Cowley, S. W. H.: Jupiter's main oval observed with HST-STIS, J. Geophys. Res., 108(A11), 1389, doi:10.1029/2003JA009921, 2003a.

Grodent, D., Clarke, J. T., Waite Jr., J. H., Cowley, S. W. H., Gérard, J.-C., and Kim, J.: Jupiter's polar auroral emissions, J. Geophys. Res., 108(A10), 1366, doi:10.1029/2003JA010017, 2003b.

Gustin, J., Gérard, J.-C., Grodent, D., Cowley, S. W. H., Clarke, J. T., and Grard, A.: Energy-flux relationship in the FUV jovian aurora deduced from HST-STIS spectral observations, J. Geophys. Res., 109, A10205, doi:10.1029/2003JA010365, 2004.

Gustin, J., Cowley, S. W. H., Gérard, J.-C., Gladstone, G. R., Grodent, D., and Clarke, J. T.: Characteristics of jovian morning bright FUV aurora from Hubble Space Telescope/Space Telescope Imaging Spectrograph imaging and spectral observations, J. Geophys. Res., 111, A09220, doi:10.1029/2006JA011730, 2006.

Hill, T. W.: Inertial limit on corotation, J. Geophys. Res., 84, 6554–6558, 1979.

Hill, T. W.: The jovian auroral oval, J. Geophys. Res., 106, 8101–8107, 2001.

Huang, T. S. and Hill, T. W.: Corotation lag of the jovian atmosphere, ionosphere and magnetosphere, J. Geophys. Res., 94, 3761–3765, 1989.

Huddleston, D. E., Russell, C. T., Kivelson, M. G., Khurana, K. K., and Bennett, L.: Location and shape of the jovian magnetopause and bow shock, J. Geophys. Res., 103, 20075–20082, 1998.

Isbell, J., Dessler, A. J., and Waite Jr., J. H.: Magnetospheric energization by interaction between planetary spin and the solar wind, J. Geophys. Res., 89, 10716–10722, 1984.

Kane, M., Mauk, B. H., Keath, E. P., and Krimigis, S. M.: Hot ions in Jupiter's magnetodisc: A model for Voyager-2 low-energy charged particle measurements, J. Geophys. Res., 100, 19473–19486, 1995.

Kennel, C. F. and Coroniti, F. V.: Is Jupiter's magnetosphere like a pulsar's or Earth's?, Space Sci. Rev., 17, 857–883, 1975.

Khurana, K. K.: Euler potential models of Jupiter's magnetic field,

J. Geophys. Res., 102, 11295–11306, 1997.

Khurana, K. K.: Influence of solar wind on Jupiter's magnetosphere deduced from currents in the equatorial plane, J. Geophys. Res., 106, 25999–26016, 2001.

Khurana, K. K. and Schwarzl, H. K.: Global structure of Jupiter's magnetospheric current sheet, J. Geophys. Res., 110, A07227, doi:10.1029/2004JA010757, 2005.

Knight, S.: Parallel electric fields, Planet. Space Sci., 21, 741–750, 1973.

Krupp, N., Lagg, A., Livi, S., Wilken, B., Woch, J., Roelof, E. C., and Williams, D. J.: Global flows of energetic ions in Jupiter's equatorial plane: First-order approximation, J. Geophys. Res., 106, 26017–26032, 2001.

Lundin, R. and Sandahl, I.: Some characteristics of the parallel electric field acceleration of electrons over discrete auroral arcs as observed from two rocket flights, in Symposium on European Rocket Research, ESA SP-135, ESA, Noordwijk, The Netherlands, p. 125, 1978.

Millward, G., Miller, S., Stallard, T., Aylward, A. D., and Achilleos, N.: On the dynamics of the jovian ionosphere and thermosphere. III. The modelling of auroral conductivity, Icarus, 160, 95–107, 2002.

Nichols, J. D. and Cowley, S. W. H.: Magnetosphere-ionosphere coupling currents in Jupiter's middle magnetosphere: Dependence on the effective ionospheric Pedersen conductivity and iogenic plasma mass outflow rate, Ann. Geophys., 21, 1419–1441, 2003,
http://www.ann-geophys.net/21/1419/2003/.

Nichols, J. D. and Cowley, S. W. H.: Magnetosphere-ionosphere coupling currents in Jupiter's middle magnetosphere: Effect of precipitation-induced enhancement of the ionospheric Pedersen conductivity, Ann. Geophys., 22, 1799–1827, 2004,
http://www.ann-geophys.net/22/1799/2004/.

Nichols, J. D., Cowley, S. W. H., and McComas, D. J.: Magnetopause reconnection rate estimates for Jupiter's magnetosphere based on interplanetary measurements at ∼5 AU, Ann. Geophys., 24, 393–406, 2006,
http://www.ann-geophys.net/24/393/2006/.

Nichols, J. D., Bunce, E. J., Clarke, J. T., Cowley, S. W. H., Gérard, J.-C., Grodent, D., and Pryor, W. R.: Response of Jupiter's UV auroras to interplanetary conditions as observed by the Hubble Space Telescope during the Cassini fly-by campaign, J. Geophys. Res., 112, A02203, doi:10.1029/2006JA012005, 2007.

Pallier, L. and Prangé, R.: More about the structure of the high latitude jovian aurorae, Planet. Space Sci., 49, 1159–1173, 2001.

Pallier, L. and Prangé, R.: Detection of the southern counterpart of the jovian northern polar cusp: Shared properties, Geophys. Res. Lett., 31, L06701, doi:10.1029/2003GL018041, 2004.

Prangé, R., Rego, D., Pallier, L., Connerney, J. E. P., Zarka, P., and Queinnec, J.: Detailed study of FUV jovian auroral features with the post-COSTAR HST faint object camera, J. Geophys. Res., 103, 20195–20215, 1998.

Radioti, A., Gérard, J.-C., Grodent, D., Bonfond, B., Krupp, N., and Woch, J.: Discontinuity in Jupiter's main auroral oval, J. Geophys. Res., 113, A01215, doi:10.1029/2007JA012610, 2008.

Rego, D., Achilleos, N., Stallard, T., Miller, S., Prangé, R., Dougherty, M., and Joseph, R.: Supersonic winds in Jupiter's aurorae, Nature, 399, 121–124, 1999.

Saur, J., Pouquet, A., and Matthaeus, W. H.: An acceleration mechanism for the generation of the main auroral oval on Jupiter, Geophys. Res. Lett., 30(5), 1260, doi:10.1029/2002GL015761, 2003.

Stallard, T., Miller, S., Millward, G., and Joseph, R. D.: On the dynamics of the jovian ionosphere and thermosphere: 1. The measurement of ion winds, Icarus, 154, 475–491, 2001.

Stallard, T. S., Miller, S., Cowley, S. W. H., and Bunce, E. J.: Jupiter's polar ionospheric flows: measured intensity and velocity variations poleward of the main auroral oval, Geophys. Res. Lett., 30(5), 1221, doi:10.1029/2002GL016031, 2003.

Southwood, D. J. and Kivelson, M. G.: A new perspective concerning the influence of the solar wind on Jupiter, J. Geophys. Res., 106, 6123–6130, 2001.

Waite Jr., J.H., Gladstone, G. R., Lewis, W. S., Goldstein, R., McComas, D. J., Riley, P., Walker, R. J., Robertson, P., Desai, S., Clarke, J. T., and Young, D. T.: An auroral flare at Jupiter, Nature, 410, 787–789, 2001.

Woch, J., Krupp, N., and Lagg, A.: Particle bursts in the jovian magnetosphere: Evidence for a near-Jupiter neutral line, Geophys. Res. Lett., 29(7), doi:10.1029/2001GL014080, 2002.

Woch, J., Krupp, N., Lagg, A., and Tomás, A.: Structure and dynamics of the jovian energetic particle distribution, Adv. Space Res., 33, 2030–2038, 2004.